Six-Prong Interactions of π^+ Mesons with Protons at 8 GeV/c

M. Bardadin-Otwinowska, T. Hofmokl, W. Wojcik, A. Wroblewski, and D. Zieminska
Institute of Experimental Physics, Warsaw University, Warsaw, Poland

and

L. Michejda,* S. Otwinowski, R. Sosnowski, and M. Szeptycka
Institute of Nuclear Research, Warsaw, Poland

(Received 19 November 1970)

Final results for 3678 six-prong π^+p events at 8 GeV/c are presented. Single-particle distributions are compared with the predictions of the Chan-Łoskiewicz-Allison model and the phenomenological model of the $F(t)$ function. Differences between the transverse momenta of the π^+ and π^- and between the transverse momenta of secondaries emitted forward and backward in the c.m. system are observed. Cross sections for production of the ρ^0, ρ^+, ρ^-, η, ω^0, X^0, and D^0 mesons and the N_{33}^{*++} and N_{33}^{*-} isobars are given, together with upper limits for some other resonances. The D^0 meson is observed in the seven-body channel in the $\eta\pi^+\pi^-$ system, with some evidence for the cascade decay $D^0 \to \delta^\pm\pi^\mp \to \eta\pi^+\pi^-$. The branching ratio $(f^0 \to 2\pi^+2\pi^-)/(f^0 \to 2\pi)$ is determined to be $(2.2^{+4.5}_{-2.2})\%$. Upper limits for the decay of A mesons into $X^0\pi$ systems are quoted. The cross section for the two-body reaction $\pi^+p \to N_{33}^{*++}X^0$ is determined to be 30 ± 13 μb, from which the η^0-X^0 mixing angle is derived. Associated production of N_{33}^{*++} and ρ^0 in the six-body channel and of N_{33}^{*++}, ρ^0, and ω^0 in the seven-body channel is studied, and the cross sections for reactions involving simultaneous production of these resonances are estimated. The Goldhaber-Goldhaber-Lee-Pais effect is studied and shown to be strong in the six-body channel, especially for selected events with low energy of the pion system.

I. INTRODUCTION

This paper contains final results of a systematic investigation of six-prong events produced by π^+ mesons of 8-GeV/c momentum interacting with protons.

In recent years there has been a growing interest of both experimentalists and theoreticians in the study of many-body reactions. Six-prong π^-p events have already been studied at 3.2,[1] 3.9,[2] 4.2,[3] 5,[4] 5.5,[5] 6,[6] 7,[7-11] 10;[12] 11,[13,14] and 16 GeV/c;[15] and π^+p events at 2.75,[16] 3.2,[17] 3.5,[17] 4,[18] 4.9,[19] 5,[20-22] 7,[23] 8,[24] and 8.5 GeV/c.[25,26] The cross section for many-prong events increases with primary momentum (Fig. 1) and one may expect that analysis of such events will be an important part of future experiments in the energy region around 50 GeV.

The progress in understanding high-multiplicity reactions has mainly been connected with the development of models in which a multiperipheral graph has been assumed together with the exchange of Regge trajectories. A model aimed at describing inelastic reactions quantitatively has been proposed by Chan, Łoskiewicz, and Allison,[27] and has been shown by the authors, and later by various experimental groups, to reproduce the main features of many-body reactions.[28]

On the other hand, some progress has also been made in the purely phenomenological studies of the transition matrix element. When examining the data, one separates phase-space effects and then tries to parametrize the matrix element using suitably chosen variables. This attempt, although less ambitious, has an advantage of not relying on theoretical concepts which contain various ambiguities and are subject to frequent changes.

In the present paper we shall discuss the predictions of the Chan-Łoskiewicz-Allison model, which we will refer to as the CŁA model, as well

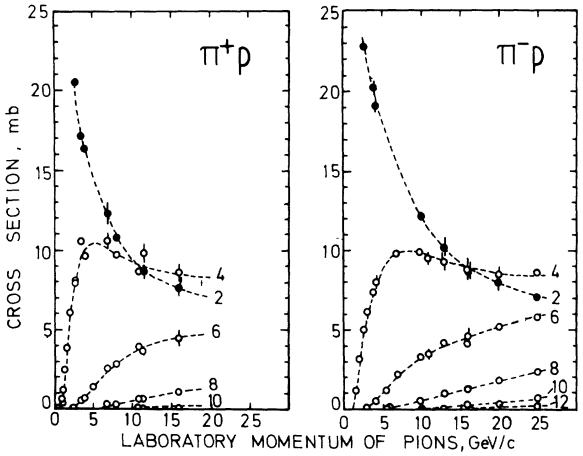

FIG. 1. Cross section for various multiplicities in π^+p and π^-p collisions below 25 GeV/c. The cross section for two-prong events includes elastic scattering. Hand-drawn curves are only to guide the eye.

as the phenomenological model of modified phase space[29] and the so-called $F(t)$ model.[30,31]

We start in Sec. III with the discussion of single-particle distributions and the comparison of the experimental results with the predictions of models. In Secs. IV and V we present results on the production of meson and baryon resonances. The production rates have been calculated with the use of the modified phase-space method,[29] which gives a good description of background in the invariant-mass distributions. Associated production of resonances is investigated in Sec. VI and the correlations of nonresonant type in Sec. VII.

Some preliminary results of this work have already been published.[24,29-35]

II. EXPERIMENTAL PROCEDURE

The photographs used in this experiment were taken in the 81-cm Saclay hydrogen bubble chamber which was exposed to the 8.04 ± 0.06-GeV/c π^+ separated beam from the CERN proton synchrotron. A scanning of 100 000 photographs yielded about

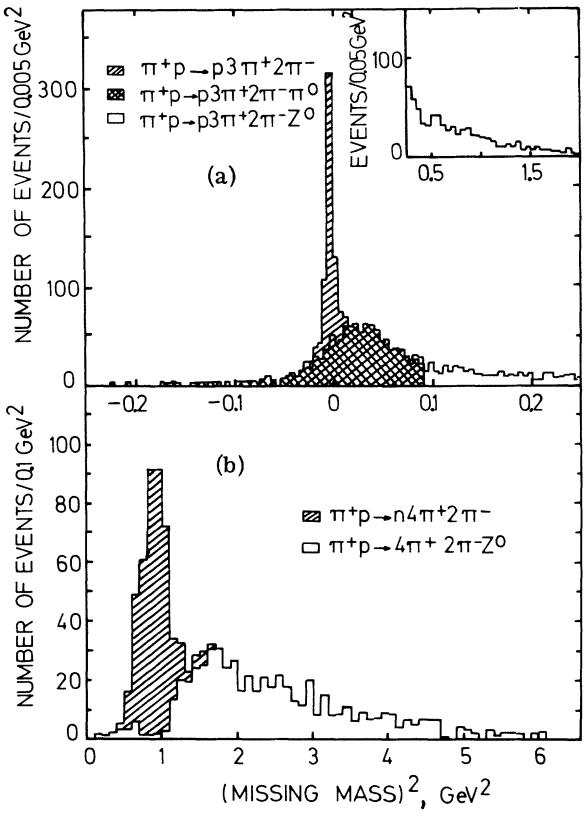

FIG. 2. Distribution of the missing mass squared as measured in this experiment: (a) for events with proton (channels A, B, and D); (b) for events of channels C and E.

4000 six-prong events. The events were measured on a MALY digitized microscope.

The geometrical reconstruction and kinematic fitting were done with the use of the Warsaw set of programs SIUP and FIT for a GIER computer.

Kinematic fits were obtained to the following reactions:

A: $\pi^+p \to p\,3\pi^+2\pi^-$,
B: $\pi^+p \to p\,3\pi^+2\pi^-\pi^0$,
C: $\pi^+p \to n\,4\pi^+2\pi^-$.

Classification of events was based on the goodness of the fit [$\chi^2 < 25$ for reaction A, $\chi^2 < 4.2$ for reactions B and C] and ionization measurements. A four-constraint (4C) fit to reaction A was always preferred to one-constraint fits to reactions B and C. In addition, events of reaction B were required to have the square of the missing mass ≤ 0.09 GeV^2. In Fig. 2(a) the distribution of the square of the missing mass is plotted for events with a proton; the hatched, cross-hatched, and unshaded histograms correspond to 4C fits, 1C fits, and no-fit events, respectively. The separation between the three seems to be quite good. Figure 2(b) shows the distribution of the square of the missing mass for events of channel C (hatched) and channel E (unshaded histogram). A distinct peak at the position of the neutron mass squared is observed

Results of identification are given in Table I.

The values of cross sections were obtained by normalization to the total cross section $\pi^+p \to 6$ prongs at this energy.[36] The errors quoted were calculated from the formula

$$\sigma = (\sigma^2_{\text{statistical}} + \sigma^2_{\text{systematic}})^{1/2}.$$

Our best estimate of $\sigma_{\text{systematic}}$ was 5% for reactions A and B and 10% for reaction C and no-fit events [reactions C and E].

The cross sections of 0.447 ± 0.031 mb for reaction A and 0.643 ± 0.052 mb for reaction B were reported at 8.5 GeV/c.[26] The latter value differs considerably from our estimate at 8 GeV/c, prob-

TABLE I. Cross sections.

Channel		Number of events	Cross section (mb)
A:	$p\,3\pi^+2\pi^-$	504	0.40 ± 0.03
B:	$p\,3\pi^+2\pi^-\pi^0$	1075	0.84 ± 0.06
C:	$n\,4\pi^+2\pi^-$	425	0.33 ± 0.04
D:	$p\,3\pi^+2\pi^-m\pi^0$, $m>1$	1093	0.86 ± 0.09
E:	$n\,4\pi^+\,2\pi^-m\pi^0$, $m\geq 1$	581	0.46 ± 0.05
	All 6 prongs	3678	2.89 ± 0.06[a]

[a]Ref. 36.

ably because of a different method of determination.

III. SINGLE-PARTICLE DISTRIBUTIONS

A. General Discussion

Simple properties of particle emission in many-body reactions may be described by single-particle distributions obtained by integration of the many-dimensional final-state momentum distribution $\Phi(\vec{p}_1, \vec{p}_2, \ldots, \vec{p}_N)$ over momenta of all particles except the one which is being studied

$$\varphi(\vec{p}_i) = \int \Phi(\vec{p}_1, \ldots, \vec{p}_N) d\vec{p}_1 d\vec{p}_2 \cdots d\vec{p}_{i-1} d\vec{p}_{i+1} \cdots d\vec{p}_N .$$

It should be remembered that single-particle distributions $\varphi(\vec{p}_i)$ allow one to reconstruct the complete distribution $\Phi(\vec{p}_1, \ldots, \vec{p}_N)$ only if correlations between particles can be neglected. Until now there has been no other experimental evidence against this hypothesis except the resonance production and the Goldhaber-Goldhaber-Lee-Pais (GGLP) effect.[37]

In the study of a single-particle distribution, one needs only two variables instead of three as a result of the azimuthal symmetry of the initial state. These variables may be chosen among such quantities as the modulus of the c.m. momentum p^*, the emission angle θ, the squared four-momentum transfer from the incident particle, t, the c.m. longitudinal momentum p_L^*, the transverse momentum p_T, etc.

Experimental two-dimensional distributions containing complete information on the production of a particle have a disadvantage of becoming obscure with a large number of entries and are not convenient for testing theoretical models. Because of that, one uses more frequently one-dimensional distributions obtained from the corresponding two-dimensional ones by integration over one of the variables. It is to be stressed, however, that an important piece of information is then lost, since, in most cases, the dependence on a pair of variables includes correlation between them.

The most suitable variable used in the discussion of single-particle distributions seems to be the c.m. longitudinal momentum p_L^*.[38] Considering this, we shall present p_L^* distributions supplemented by the distributions of the transverse momentum p_T, and the p_T vs p_L^* plots, which show a correlation between the transverse and longitudinal momenta. Furthermore, we shall discuss the squared four-momentum transfer t, from the initial proton to the secondary nucleon.

B. On the Use of Phase Space

The final-state momentum distribution $\Phi(\vec{p}_1, \ldots, \vec{p}_N)$ can be expressed in the form:

$$\Phi(\vec{p}_1, \ldots, \vec{p}_N) d\vec{p}_1 \cdots d\vec{p}_N = |S|^2 \delta(E - \sum E_i)\, \delta(\sum \vec{p}_i)\, \frac{d\vec{p}_1}{E_1} \cdots \frac{d\vec{p}_N}{E_N} ,$$

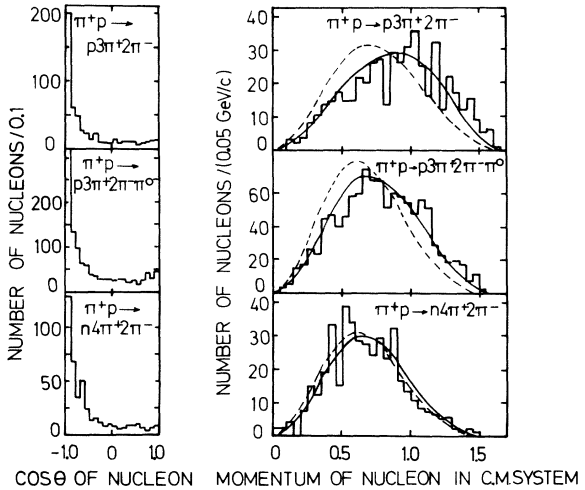

FIG. 3. Distributions of the c.m. emission angle and c.m. momentum of nucleons in channels A, B, and C. Relativistic phase-space curves are shown by dashed lines and predictions of the $F(t)$ model by solid lines.

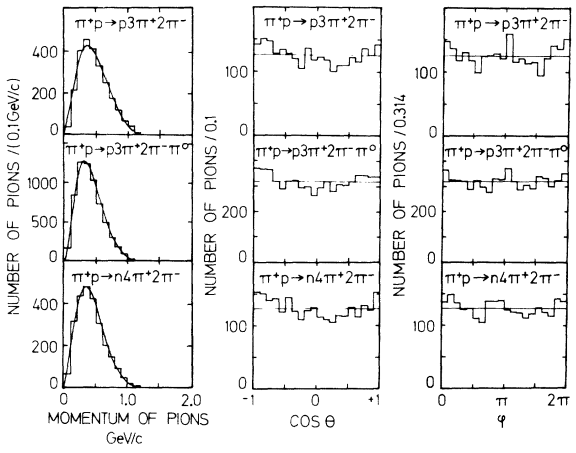

FIG. 4. Distributions of the momentum and emission angles of pions in the rest system of all pions. The emission angles θ and φ are defined in the reference frame in which the z axis is antiparallel to the momentum vector of the secondary nucleon transformed to the rest system of all pions, and the y axis is along the normal to the nucleon production plane. Solid lines show the prediction of the relativistic phase space calculated in the rest system of all pions and weighted according to the experimental c.m. momentum distribution of the nucleon.

where S is the transition-matrix element.

It is well known that interactions at high energy cannot be described by the phase space alone ($|S|^2 = 1$). This fact is illustrated in Fig. 3, which shows the distributions of the c.m. momentum and emission angle of the nucleon for reactions A, B, and C. The phase-space curves (dashed lines) fail to reproduce the momentum distributions of protons and a very pronounced backward peaking is observed in all three angular distributions. This demonstrates the importance of the transition-matrix element in the description of the emission of nucleons, and rules out the possibility of using phase space even as a first approximation. Nevertheless it seems to us that in the interactions studied in this work, the phase space could be used for the description of the subsystem of all pions.

Figure 4 shows that in the rest frame of all pions the distributions of the emission angles of pions are nearly isotropic, with the $\cos\theta$ distributions showing a small excess of pions emitted in the forward and backward directions. θ is the angle between the pion momentum vector and the vector opposite to the direction of the outgoing nucleon; θ is transformed to the rest system of all pions, in analogy to the helicity frame for the two-body reactions. However, if one uses the direction of the incoming pion transformed to the rest frame of all pions to define the emission angle θ' (like the Jackson angle), then the distribution of $\cos\theta'$ (not shown) is more peaked at $|\cos\theta'| \approx 1$. This indicates that the pionic cloud is elongated rather in the direction of the incoming pion than in the direction of the outgoing nucleon.

The momentum distributions of pions in Fig. 4 agree well with the predictions of relativistic phase space applied to the subsystem of pions only. In the calculation, the spectrum of the total energy of the pionic system was taken from experiment.

We conclude that to a fairly good approximation, the pionic system can be described by the relativistic phase space, therefore the matrix element depends mostly on nucleon variables.

These features have already been discussed in Ref. 33.

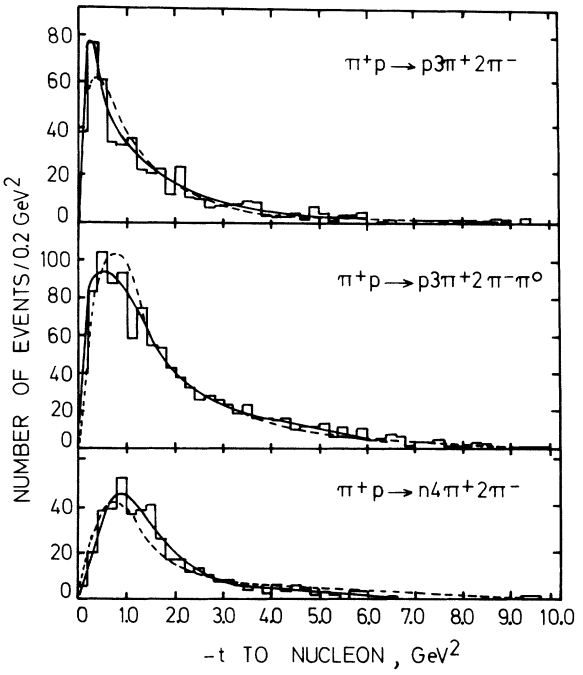

FIG. 5. Distribution of the squared four-momentum transfer, t, to nucleon for channels A, B, and C. Solid lines represent the distributions smoothed out by the $F(t)$ function, dashed lines are calculated from the CLA model.

C. Four-Momentum-Transfer Distributions and The $F(t)$ Model

The distributions of the squared four-momentum transfer, t, from the initial to the final nucleon for channels A, B, and C are shown in Fig. 5. They are correctly reproduced by the multi-Regge-exchange model of Chan *et al.*[27] (dashed lines). In this work we used the same set of parameters as given by the authors in Ref. 27.

When one compares the t distributions of high-multiplicity interactions with those of low-multiplicity or two-body reactions, one would like to remove the influence of phase space, which differs from one channel to another. Therefore we calculated the function $F(t)$, introduced by Białkowski and Sosnowski,[30] defined as the ratio of the experimental t distribution to the phase-space t distribution:

$$F(t) = \frac{N(t)_{\text{experimental}}}{N(t)_{\text{phase space}}} .$$

The functions $F(t)$ for channels A, B, and C are plotted in Fig. 6. They were fitted (full lines) with the formula

$$F(t) \sim e^{at} + be^{ct} + d,$$

TABLE II. Coefficients of the fitted $F(t)$ function, $F(t) \sim e^{at} + be^{ct} + d$.

Channel	Coefficients a (GeV^{-2})	b	c (GeV^{-2})	d
$p\,3\pi^+2\pi^-$	7.1 ± 1.0	0.044	1.45	1.94×10^{-3}
$p\,3\pi^+2\pi^-\pi^0$	10.1 ± 1.5	0.054	1.83	1.74×10^{-3}
$n\,4\pi^+2\pi^-$	17.1 ± 11.6	0.097	1.57	1.75×10^{-3}

TABLE III. Average transverse momenta of nucleons in MeV/c.

Channel	Experiment	Relativistic phase space	$F(t)$ model	CLA model
A	p: 441±10	591	425	436
B	p: 435± 7	520	416	426
C	n: 382± 9	520		
D	p: 388± 6			
E	Z^0: 428± 9[a]			

[a] Z^0 stands for the missing neutral system, which for channel E consists of a neutron and one or more π^0's.

and the obtained values of the coefficients are given in Table II. It may be noted that the values of the coefficient a, i.e., of the slope of the function $F(t)$ in the region of small t, are of the order of 10 GeV^{-2}, similar to those observed in two-body reactions.[36] The fits obtained multiplied by the curves $N(t)_{\text{phase space}}$ are reproduced (solid lines) in the initial t distributions in Fig. 5.

It has been shown in Ref. 30 that a matrix element depending only on the four-momentum transfer from the initial to the final nucleon is sufficient to reproduce the main features of particle emission in the interactions studied. Any additional dependence of the matrix element on nucleon variables other than t was proven to be weak.[31] For example, in the Chew-Low plot of p^* vs t (not shown), the distribution of points along the p^* axis (t=const) is consistent with phase space.

The phenomenological model in which it is assumed that the matrix element can be replaced by the $F(t)$ function will be refered to as the $F(t)$ model.

D. Longitudinal and Transverse Momentum of Nucleons

The c.m. longitudinal- and transverse-momentum distributions of protons from channels A and B are shown in Fig. 7. They are well reproduced by both the $F(t)$ model (solid lines) and the CLA model (dashed lines). The values of the average transverse momentum $\langle p_T \rangle$ of nucleons are collected in Table III and compared with the predictions of the CLA and $F(t)$ models for channels A and B. In Tables IV and V are given the average values of the c.m. longitudinal momentum $\langle p_L^* \rangle$ of nucleons and the values of the ratio $(F-B)/(F+B)$, where F and B are the numbers of particles with $p_L^* > 0$ and $p_L^* < 0$, respectively.

In Fig. 8 the values of $\langle p_T \rangle$, calculated for various intervals of p_L^*, are plotted as a function of p_L^* and compared with the predictions of the $F(t)$ model (solid lines) and the CLA model (dashed lines). In both models the predicted values of $\langle p_T \rangle$ are higher for the protons emitted forwards than for those emitted backwards, in agreement with the tendency observed in experimental data. The curve of the CLA model follows the data better.

TABLE IV. Average c.m. longitudinal momenta in MeV/c.

Channel	p or n	π^+	π^-	π^0
A	−571±26	101±11	132±12	•••
B	−376±17	49±6	75±7	84±10
C	−407±20	88±9	29±10	•••

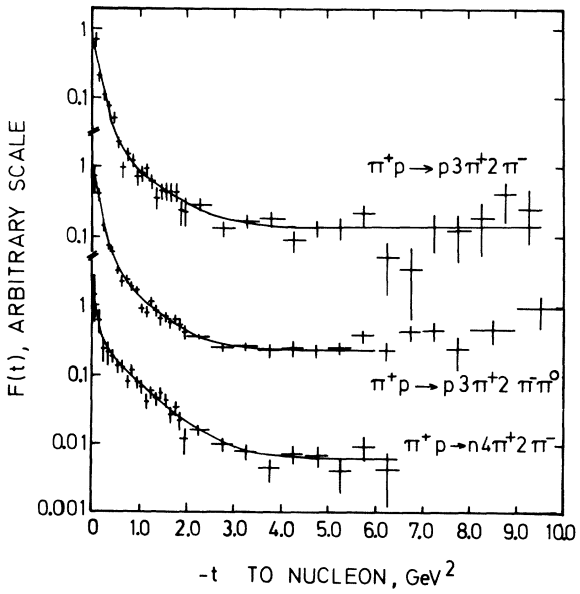

FIG. 6. $F(t)$ functions for channels A, B, and C. The parametrization of the solid lines is given in Table II.

TABLE V. $(F-B)/(F+B)$ ratios.

Channel	p or n	π^+	π^-	π^0
A	-0.63 ± 0.04	0.13 ± 0.03	0.26 ± 0.03	•••
B	-0.50 ± 0.03	0.07 ± 0.02	0.19 ± 0.02	0.21 ± 0.03
C	-0.70 ± 0.05	0.14 ± 0.02	0.05 ± 0.03	•••

E. Longitudinal Momentum of Pions

1. *Comparison with Models*

The predictions of the CL̸A and $F(t)$ models have already been compared in Refs. 27 and 31 with our experimental p_L^* distributions summed over all pion charges. In Fig. 9 we reproduce our data for channel A and the curves predicted by both models. The CL̸A model predicts too much elongation, i.e., too many pions in the tails of the p_L^* distribution.

On the contrary, the $F(t)$ model predicts too few pions in the very forward direction. This is a consequence of the fact that the spherical symmetry of pions in the rest system of all pions, assumed in the $F(t)$ model, is only approximately correct (Sec. III B).

The differences between the predictions of both models and the data, observed in the p_L^* distributions, are reflected in the average values of the transverse momentum of pions, which will be discussed in Sec. III F 1.

2. *Difference Between π^+ and π^-*

The CL̸A and $F(t)$ models discussed here are not able to distinguish between pions of different charge. Despite that we shall compare the experimental p_L^* distributions of π^+ and π^- because the differences between them may give some hints as to the production mechanism.

The c.m. longitudinal-momentum distributions of

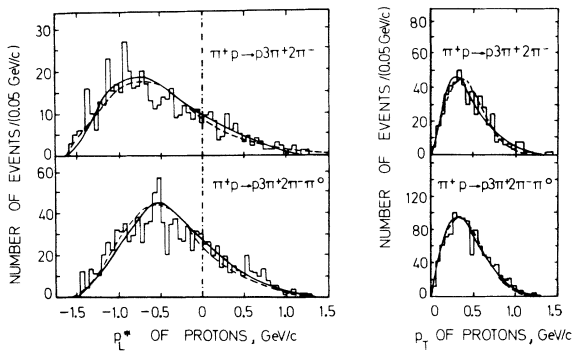

FIG. 7. Longitudinal and transverse momentum distributions of protons from channels A and B compared with the curves predicted from the $F(t)$ model (solid lines) and the CL̸A model (dashed lines).

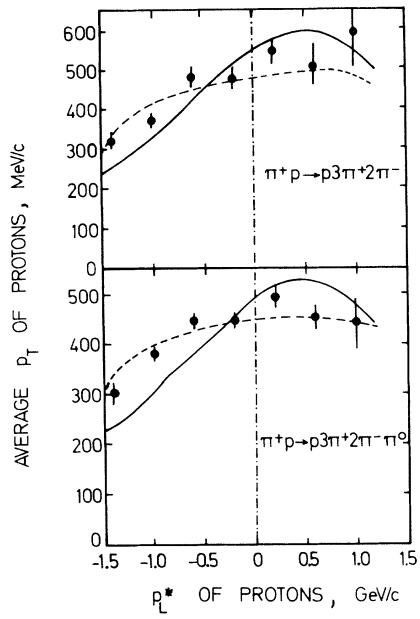

FIG. 8. Dependence of the average transverse momentum $\langle p_T \rangle$ on the longitudinal c.m. momentum p_L^* of protons in channels A and B. Solid lines show the prediction of the $F(t)$ model and dashed lines the prediction of the CL̸A model.

π^+ and π^- from channels A and B are shown in Fig. 10. In the π^+ distributions pions from the N_{33}^{*++} decay[39] (shaded area) are grouped around $p_L^* \approx -50$ MeV/c. The π^- distributions were approximated with curves which were then normalized to the number of positive pions which do not originate from the N^{*++} decay, and are repeated in the corresponding π^+ distributions.

We note a small excess of positive pions emitted very forward which may suggest that the effect of

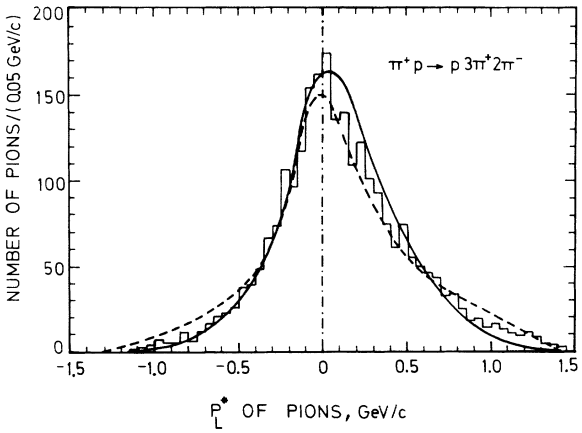

FIG. 9. Distribution of the longitudinal c.m. momentum for all pions in channel A. Prediction of the $F(t)$ model is shown by solid line and that of the CL̸A model by dashed line.

a "leading pion" is present but weak. In addition, the distribution of all positive pions is shifted backward with respect to the distribution of negative pions.

The average values of p_L^* for the fitted channels are given in Table IV. In channels A and B they are lower for π^+ mesons (i.e., beamlike pions) than for the π^- mesons. This rather unexpected result, not observed in channel C, is partly due to the presence of N^{*++} (see also Ref. 20). However, the average p_L^* of the π^+ mesons from the N^{*++} decay, equal to -104 MeV/c for channel A and -61 MeV/c for channel B, is not sufficiently different from the over-all average to explain fully this phenomenon. After removing pions from the N^{*++} decay, the values of $\langle p_L^* \rangle$ of the remaining positive pions are equal to 122 MeV/c (channel A) and 66 MeV/c (channel B) and despite the forward excess of the π^+, are not higher than those for π^-, 132 MeV/c (channel A) and 75 MeV/c (channel B).

The forward excess of the positive pions and their backward shift may be qualitatively explained in the multiperipheral model in the following manner: A negative pion cannot be emitted from the incident π^+ vertex, nor from the baryonic vertex, if the exchange of doubly charged baryons in neglected. However, this conjecture expressed in terms of the CLA model cannot quantitatively explain the data, as has been verified in Ref. 40. One may note that the total charge of all pions equals +1, and the forward emission of neutral ρ and ω mesons (see Sec. IV C 1) may be related to the backward shift of the positive charge.

For the sake of completeness, the coefficients $(F-B)/(F+B)$ are collected in Table V for fitted channels.

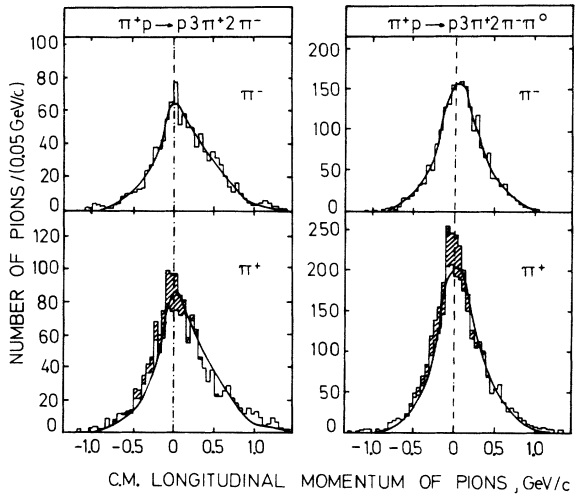

FIG. 10. Distribution of the longitudinal c.m. momentum p_L^* for π^- and π^+ in channels A and B (see text for detailed explanation).

F. Transverse Momenta of Pions

1. Experimental Data and Comparison with Models

The distributions of the transverse momentum of pions for channels A and B are shown in Fig. 11 and compared with the predictions of the CLA (dashed lines) and the $F(t)$ model (solid lines). The values of the average transverse momentum of pions for all channels are given in Table VI. The values of Ref. 33 are obtained with the modified phase-space method (Sec. IV A) but including the contribution of pions from N^{*++} decay.

The $F(t)$ model predicts too high transverse momenta of pions, whereas the CLA model predicts too low p_T values. This is again related to the fact that the distribution of pions in their rest frame is not exactly spherically symmetric as required by the $F(t)$ model, but less elongated than it follows from the CLA model. These discrepancies are also seen in Fig. 12, where the average transverse momentum of the pions (all charges) is plotted against their longitudinal momentum for channels A and B. The dip at $p_L^*=0$ originating simply from the relativistic phase space[41] is observed and reproduced by the CLA model (dashed lines) and the $F(t)$ model (solid lines), however, the position of the curve is too low for the former and too high for the latter.

A better description of the data by the CLA model could probably be achieved by a readjustment of the model parameters, which we did not attempt.

There is experimental evidence for a difference between the values of $\langle p_T \rangle$ for pions in the forward and backward hemisphere: For channel A the forward average is $\langle p_T \rangle_F = 357 \pm 5$ MeV/c and the back-

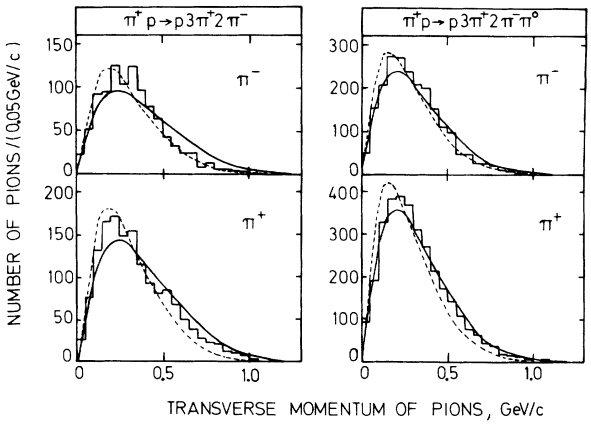

FIG. 11. Distributions of the transverse momentum of π^- and π^+ from channels A and B compared with the predictions of the $F(t)$ model (solid lines) and the CLA model (dashed lines).

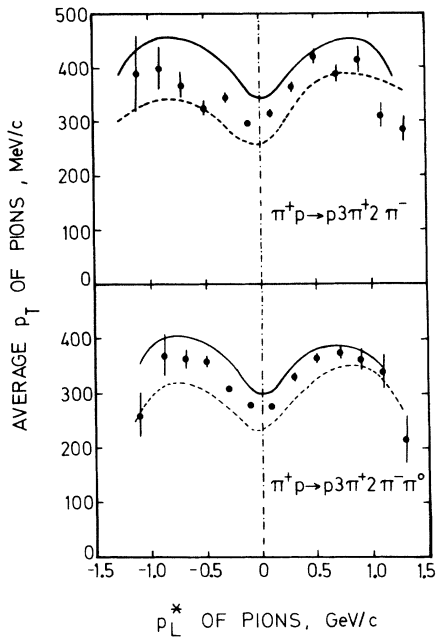

FIG. 12. Dependence of the average transverse momentum $\langle p_T \rangle$ on the longitudinal c.m. momentum p_L^* of pions in channels A and B. Solid lines show predictions of the $F(t)$ model and dashed lines the predictions of the CLA model.

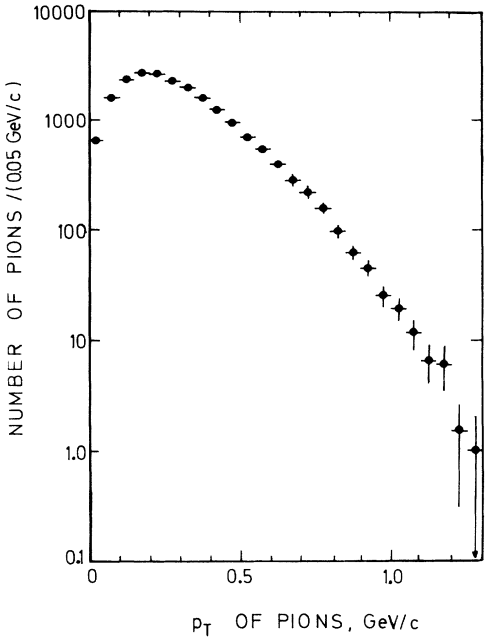

FIG. 13. Distribution of the transverse momentum for all pions measured in this experiment (20 471 particles).

ward average is $\langle p_T \rangle_B = 321 \pm 5$ MeV/c; for channel B the corresponding values are $\langle p_T \rangle_F = 314 \pm 3$ MeV/c and $\langle p_T \rangle_B = 297 \pm 3$ MeV/c.

The distribution of the transverse momentum of 19 396 charged pions from channels A, B, C, D, and E and of 1075 neutral pions from channel B is plotted in logarithmic scale in Fig. 13. The average transverse momentum is equal to 291±1 MeV/c; the corresponding value at 5 GeV/c is lower and equal to 253 ±1 MeV/c.[20]

2. *Comparison of Beam-Like and Beam-Unlike Pions*

We notice that in our experiment the $\langle p_T \rangle$ values are always higher for positive pions than for the negative ones. The difference is very clear for channels without protons and therefore without N^{*++}, which is a source of π^+ with low transverse momentum. The values of $\langle p_T \rangle$ for beam-like-charge pions, beam-unlike-charge pions, and protons from six- and seven-body interactions are collected in Table VII. They are plotted in Fig. 14 as a function of the total c.m. energy divided by the number of secondary particles. This procedure allows us to bring the $\langle p_T \rangle$ points from six- and seven-body channels onto a common curve, especially in the region near the threshold.

It is evident from Fig. 14 that the transverse momentum of beam-like-charge pions is systematically higher than that of pions of opposite charge. As one can see from Table VII, in the $\pi^- p$ interactions the effect is even stronger, probably because of the low transverse momentum of the π^+ from N^{*++} decay which contributes to the difference,

TABLE VI. Average transverse momenta of pions in MeV/c.

Channel	Experiment π^+	π^-	π^0 or Z^0	All pions	Relativistic phase space	Model of Ref. 33	$F(t)$ model	CLA model
A	351±4	329±5	•••	342±3	414	353	388	308
B	317±3	304±3	284±4	307±2	348	312	333	275
C	334±4	279±5	•••	316±3	348			
D	259±3	245±3	351±6[a]					
E	279±4	246±5	•••					

[a] Z^0 stands for the missing neutral system, which for channel D consists of two or more π^0's.

whereas in the case of incident π^+ some cancellation may be expected.

IV. MESONIC RESONANCES

A. Modified Phase-Space Method

It has been shown in Sec. III that the matrix element involved in the interactions studied in this work strongly depends on nucleon variables, whereas the subsystem of all pions can be described to a good approximation by the phase space.

The effective-mass distribution of any system of particles is therefore determined by the distribution of one variable only, namely of the modulus of the c.m. momentum of protons which may be taken from the experiment.

This approach, called the modified phase-space method, would be a direct consequence of the $F(t)$ model if the latter correctly predicted the nucleon c.m. momentum distribution. In fact, the agreement is not perfect (see Fig. 3). Therefore, one expects a more accurate description of the effective-mass distributions when one inserts the experimental c.m. momentum distribution of nucleons instead of that calculated from the $F(t)$ model.

In channel C the c.m. momentum distribution of neutrons agrees with the phase-space predictions; therefore, effective-mass distributions in this channel have been calculated from the phase space without modifications.

A detailed description of the modified phase-space method and the comparison with experimental mass distributions have been reported previously.[29] It has been shown there that in our experiment the modified phase space reproduces quantitatively the effective-mass distributions of mesonic systems of any number of pions of any charge.

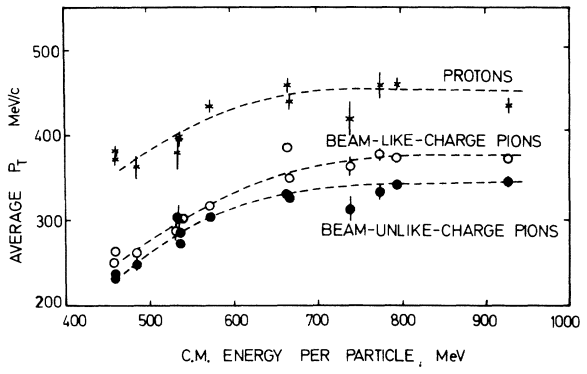

FIG. 14. Average transverse momenta of protons (×), beam-like-charge pions (○), and beam-unlike-charge pions (●) from six- and seven-body $\pi^{\pm}p$ interactions as a function of c.m. energy divided by the number of secondary particles. The values of $\langle p_T \rangle$ are given in Table VII. Hand-drawn curves are only to guide the eye.

B. Cross Sections

In high-multiplicity events the background under a resonance peak is usually large and the estimate of the cross section depends strongly on the assumed shape of the background.

In our case, we used the predictions of the modified phase space including reflections of the ρ^0 production in channel A and of the ρ^0, ρ^+, ρ^-, ω^0, and η^0 production in channel B. This background, and Breit-Wigner formulas for resonances, were fitted to the experimental histograms in the whole mass region. In all fits a good χ^2 probability was obtained.

1. ρ Production

In order to estimate the ρ production, we used the relativistic Breit-Wigner formula with a mass-dependent width[42]:

$$d\sigma \sim \frac{\Gamma}{(m^2 - m_0^2)^2 - \Gamma^2 m_0^2}\,\Phi(m)\,dm\,,$$

where

$$\Gamma(m) = \Gamma(m_0)\frac{m_0}{m}\left(\frac{q}{q_0}\right)^3 .$$

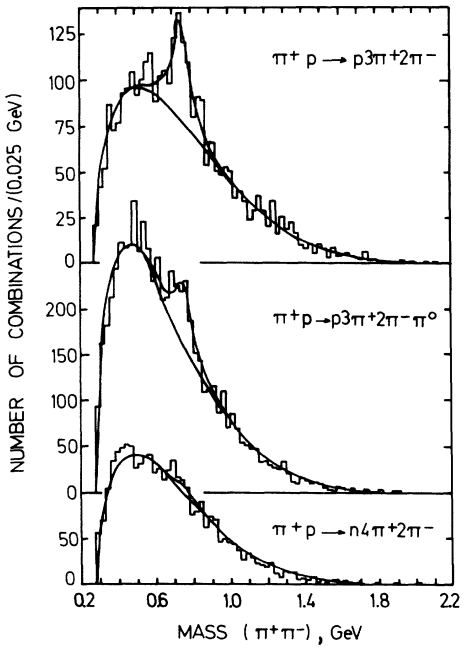

FIG. 15. Effective-mass distributions of the $\pi^+\pi^-$ system in channels A, B, and C. The upper solid lines show the results of the fit with a sum of the Breit-Wigner distribution and the modified phase-space curve shown below.

Here m_0 and $\Gamma(m_0)$ are the intrinsic mass and width of the ρ, m denotes the mass of the $\pi\pi$ system, q is the momentum of the pion in the rest frame of the $\pi\pi$ system, and q_0 is the value of q at $m = m_0$. The function $\Phi(m)$ is the relativistic phase-space integral for a system composed of one particle with mass m and $k-2$ pions, where k is the number of pions produced in the interactions. In all fits, the mass and width of the ρ meson were fixed, $m_0 = 756$ MeV and $\Gamma(m_0) = 115$ MeV.

The effective-mass distributions of the $\pi^+\pi^-$ system and the fitted curves for reactions *A*, *B*, and *C* are shown in Fig. 15. The ρ^0 meson is copiously produced in reactions *A* and *B* with the production rates of $(66 \pm 8)\%$ and $(38 \pm 5)\%$, respectively, whereas in reaction *C* the fit gives $(10 \pm 10)\%$ for the production rate of ρ^0. By production rate we mean the ratio of the number of combinations in a resonance peak to the total number of events.

In Figs. 16(a) and 16(b) the distributions are presented of the effective mass of the $\pi^-\pi^0$ and $\pi^+\pi^0$ systems, respectively. The production rates are estimated to be $(6 \pm 3)\%$ for ρ^- and $(10 \pm 3)\%$ for ρ^+ mesons.

In order to illustrate the importance of the correct estimate of the background, the experimental histogram of $\pi^+\pi^0$ effective mass is repeated in Fig. 16(c) and compared with the modified phase-space curve without reflections of resonance production. This shape of background leads to an estimate of production rate consistent with zero, whereas a three-standard-deviation effect is detected if the correct shape of background is used. The difference between the two background curves is mainly due to the reflection of the ω and η production which enhances the region of low $\pi^+\pi^0$ masses.

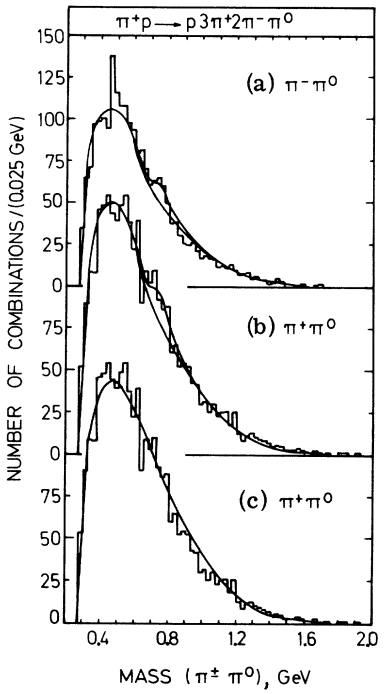

FIG. 16. (a) and (b) Effective-mass distributions of $\pi^-\pi^0$ and $\pi^+\pi^0$ systems in channel *B*. The upper solid lines show the results of the fit with a sum of the Breit-Wigner curve and the modified phase-space curve shown below. (c) The same histogram as in (b) compared with the modified phase-space curve without reflections.

2. ω and η Production

The $\pi^+\pi^-\pi^0$ effective-mass distribution, presented in Fig. 17, was fitted with a sum of the modified phase-space background and two Breit-Wigner formulas. The mass and width of the η were fixed at the values of 549 MeV and 46 MeV, respectively. For the ω, the following values were obtained from the fit: $M = 784 \pm 4$ MeV and $\Gamma = 45 \pm 8$ MeV, uncorrected for experimental resolution. The ω meson is produced in $(31 \pm 4)\%$ and η in $(3 \pm 1)\%$ of the interactions. The corresponding cross sections, corrected for unseen decay modes,[43,44] are 0.29 ± 0.04 and 0.09 ± 0.03 mb, respectively. Events with X^0 production (see below) were not included in Fig. 17, nor in the above estimates of the frequency and cross section for η production.

3. X^0 Production

The effective-mass distribution of the $\pi^+\pi^+\pi^-\pi^-\pi^0$ system is plotted in Fig. 18; the histogram 18(a) contains all combinations and 18(b) those having

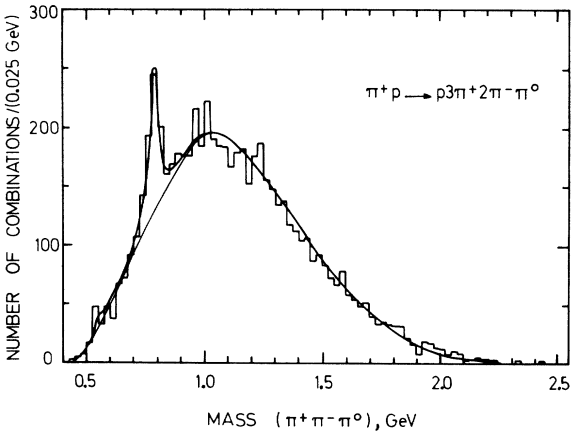

FIG. 17. Effective-mass distribution of the $\pi^+\pi^-\pi^0$ system in channel *B*. The upper solid line show the result of the fit with a sum of two Breit-Wigner curves and the modified phase-space curve shown below.

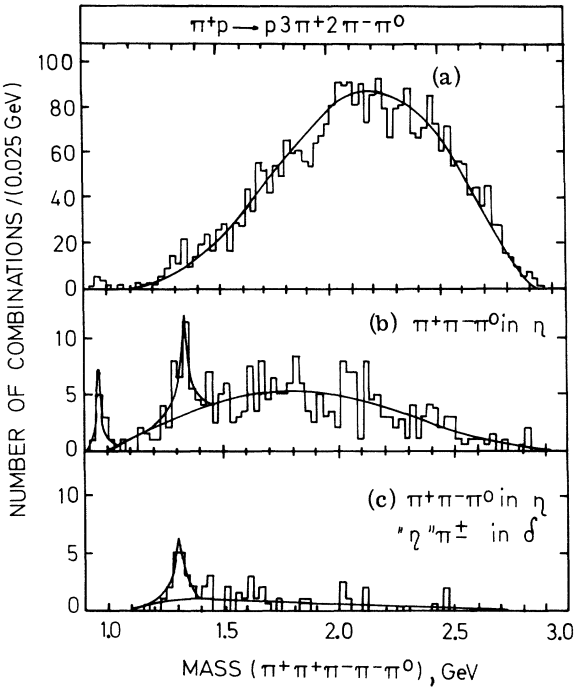

FIG. 18. Effective-mass distribution of the $\pi^+\pi^+\pi^-\pi^-\pi^0$ system in channel B: (a) All combinations. The solid line is the prediction of the modified phase space. (b) Under the condition that at least one $\pi^+\pi^-\pi^0$ combination has the mass in the η band (0.5–0.6 GeV). The upper solid line shows the result of the fit with a sum of two Breit-Wigner distributions and the modified phase-space background shown below. (c) Under the same conditions as in (b), and with the mass of the "η'π^+ or "η'π^- system in the δ band (0.925–0.975 GeV). The upper solid line is the result of the fit with the Breit-Wigner curve and the modified phase-space background shown below.

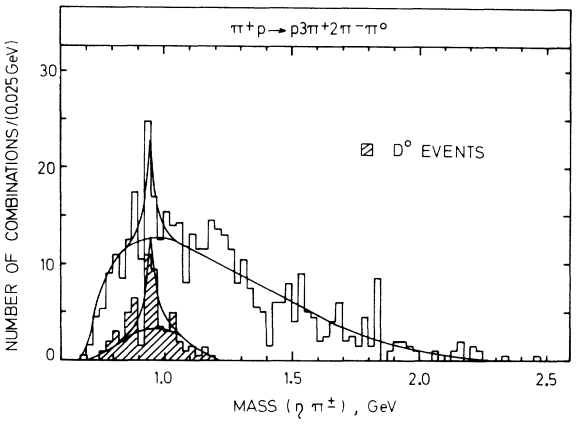

FIG. 19. The $\pi^+\pi^-\pi^0\pi^\pm$ effective-mass distribution with at least one $\pi^+\pi^-\pi^0$ combination in the η band. The shaded area corresponds to the selected D^0 events [1.275 $< M(\pi^+\pi^+\pi^-\pi^-\pi^0) <$ 1.375 GeV]. The upper curves show the results of the fits with the Breit-Wigner formula and the modified phase-space background shown below.

TABLE VII. Average transverse momenta in MeV/c for reactions $\pi p \to p5\pi$ and $\pi p \to p6\pi$ for various incident pion momenta. The values of the difference between $\langle p_T \rangle$ of pion with charge of the beam and $\langle p_T \rangle$ of pion with opposite charge, Δp_T, are also given.

Charge and momentum of incident pion	Reference	Reaction $\pi^\pm p \to p\pi^+\pi^+\pi^-\pi^-$				$\frac{1}{6}E^{\text{c.m.}}$ (MeV)	Reaction $\pi^+ p \to p\pi^+\pi^+\pi^-\pi^-\pi^0$					$\frac{1}{7}E^{\text{c.m.}}$ (MeV)
		p	π^+	π^-	Δp_T		p	π^+	π^-	Δp_T		
π^+, 4 GeV/c	21	363 ± 14	263 ± 5	249 ± 7	14 ± 9	484	...	...	...	...	...	...
π^-, 5 GeV/c	4	397 ± 7	273 ± 4	302 ± 4	29 ± 6	535	382 ± 7	232 ± 3	251 ± 3	19 ± 4		459
π^+, 5 GeV/c	20	396 ± 10	286 ± 4	286 ± 5	0 ± 6	535	372 ± 8	265 ± 3	237 ± 4	28 ± 5		459
π^-, 7 GeV/c	7	...	...	...	...	...	380 ± 20	303 ± 16	289 ± 14	−14 ± 21		536
π^+, 8 GeV/c		441 ± 10	351 ± 4	329 ± 5	22 ± 6	666	435 ± 7	317 ± 3	304 ± 3	13 ± 4		571
π^-, 10 GeV/c	12	420 ± 20	314 ± 14	365 ± 11	51 ± 18	738	...	...	...	...		...
π^-, 11 GeV/c	13	460 ± 16	334 ± 8	376 ± 8	42 ± 11	774	460 ± 9	331 ± 5	389 ± 4	58 ± 6		664
π^-, 16 GeV/c	15	436 ± 10	346 ± 5	373 ± 5	27 ± 8	927	461 ± 7	344 ± 4	375 ± 3	31 ± 5		794

TABLE VIII. Production rates and cross sections for mesonic resonances. The cross sections are corrected for unseen decay modes. Errors correspond to 68% confidence level.

Channel	Resonance	8 GeV/c %	8 GeV/c σ (mb)	5 GeV/c[a] %	5 GeV/c[a] σ (mb)	4 GeV/c[b] %	4 GeV/c[b] σ (mb)
$p\,3\pi^+2\pi^-$	ρ^0	66.3 ± 8.3	0.265 ± 0.039	63 ± 12	0.26 ± 0.05	...	...
$p\,3\pi^+2\pi^-\pi^0$	ρ^0	38.1 ± 5.2	0.320 ± 0.049	<4.9[c]	<0.03[c]	...	...
	ρ^+	10.3 ± 3.4	0.086 ± 0.029	<3.3[c]	<0.02[c]	...	...
	ρ^-	6.3 ± 2.7	0.053 ± 0.023	<2.5[c]	<0.015[c]	...	...
	ω	30.6 ± 4.0	0.289 ± 0.043	42 ± 4	0.29 ± 0.03	62 ± 4	0.174 ± 0.26
	η	3.1 ± 1.2[d]	0.090 ± 0.035[d]	4.4 ± 1	0.093 ± 0.019	11 ± 3	0.091 ± 0.030
	X^0	0.9 ± 0.3	0.060 ± 0.019	1.0 ± 0.3	0.046 ± 0.019	5 ± 1.7	0.098 ± 0.035
	D^0	2.3 ± 0.6	0.066 ± 0.017[e]	...	...	...	...
$n\,4\pi^+2\pi^-$	ρ^0	10.4 ± 9.4	0.034 ± 0.031	...	...	...	...

[a]Ref. 20.
[b]Ref. 18.
[c]Upper limits are calculated with confidence level of 95%.
[d]η produced through the X^0 meson is excluded.
[e]Calculated for $D^0\to\eta\pi^+\pi^-$.

at least one combination in the η band defined as $500<M(\pi^+\pi^-\pi^0)<600$ MeV. In both histograms a peak containing 10 events is observed at the position of the X^0 meson, whereas the background of nonresonant combinations below 1025 MeV is estimated to be less than one event. A maximum-likelihood fit to the X^0 events gives the value of mass $M=965\pm4$ MeV and width $\Gamma=22^{+12}_{-7}$ MeV. The value of Γ is consistent with our experimental resolution. The cross section corresponding to 10 observed events is 7.8 ± 2.5 μb. After the correction[45] for unseen decay modes of X^0 and η^0, the value of 60 ± 19 μb is obtained.

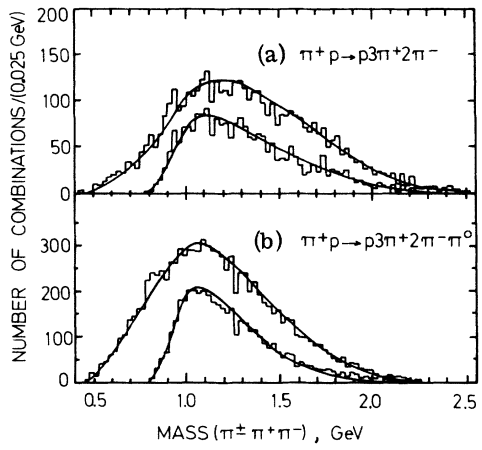

FIG. 20. Effective-mass distributions of $\pi^+\pi^-\pi^\pm$ system in channels A and B. Lower histograms in Figs. 20(a) and 20(b) are obtained under the condition that at least one $\pi^+\pi^-$ mass is in the ρ band. Solid lines show the predictions of the modified phase space.

4. D^0 Production

In the "η"$\pi^+\pi^-$ mass distribution presented in Fig. 18(b), an excess of events is observed at the position of the D^0 meson with a statistical significance of four standard deviations. It has been checked[46] that the excess is correlated with the resonant η combinations. A very good fit was obtained to the whole region of the "η"$\pi^+\pi^-$ mass above 1025 MeV with the relativistic Breit-Wigner formula and the modified phase-space background. The fitted D^0 mass is $M=1329\pm10$ MeV and width $\Gamma=52\pm29$ MeV. The number of events, 24 ± 6, corresponds to a cross section of 66 ± 17 μb, cor-

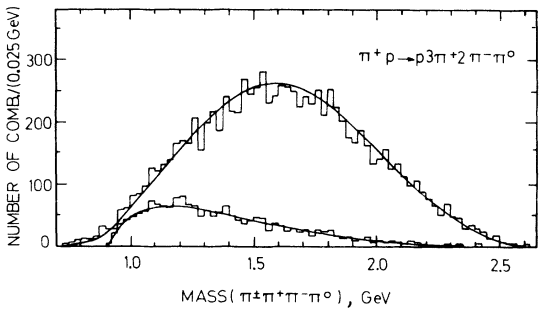

FIG. 21. Effective-mass distributions of $\pi^+\pi^-\pi^0\pi^\pm$ system in channel B. Solid lines are the predictions of the modified phase space. Lower histogram shows the $\pi^+\pi^-\pi^0\pi^\pm$ mass distribution under the condition that at least one $\pi^+\pi^-\pi^0$ mass is in the ω band.

rected for unseen decay modes of η.

The effective-mass distribution of the "η"$\pi^\pm$ system (upper histogram in Fig. 19) shows some enhancement at the mass of the δ meson. After selection of the "η"$\pi^\pm$ combinations for which the "η"$\pi^+\pi^-$ mass is in the D^0 region from 1275 to 1375 MeV, the background is considerably reduced, whereas the signal of δ is only slightly lowered. A fit with the Breit-Wigner formula and the modified phase-space background to the lower histogram gives the values of δ mass 947 ±7 MeV, width 31 ±28 MeV, and the number of events in the peak 21 ±7. The calculated background includes the ω reflection which was demonstrated[47] to have a negligible effect.

The data presented indicate that the decay of D^0 into $\eta\pi^+\pi^-$ involves an intermediate two-body decay into $\delta^\pm\pi^\mp$.[48]

Assuming that the observed three-standard-deviation signal is due to the δ meson, we have plotted in Fig. 18(c) the effective-mass distribution of the $\pi^+\pi^+\pi^-\pi^-\pi^0$ system containing "η", i.e., at least one $\pi^+\pi^-\pi^0$ combination in the η band, and "δ", i.e., the "η"$\pi^\pm$ in the δ band between 925 and 975 MeV. If the assumption is true, then the values $M = 1303 \pm 8$ MeV and $\Gamma = 44 \pm 24$ MeV obtained from the fit to the histogram in Fig. 18(c) should be considered as our best estimates of the mass and width of the D^0 meson.

The above values of width of the D^0 and δ mesons are not corrected for experimental resolution.

TABLE IX. Upper limits of cross sections for production of mesonic resonances, uncorrected for unseen decay modes. The upper limits at 8 GeV/c are calculated with confidence level of 68%, at 5 GeV/c with confidence level of 95%.

		σ (mb)	
Channel	Resonance	8 GeV/c	5 GeV/c[a]
$p\,3\pi^+\,2\pi^-$	$A_1^+ + A_1^-$	<0.025	<0.03
	$A_2^+ + A_2^-$	<0.03	<0.02
	f^0	<0.02	<0.005
$p\,3\pi^+\,2\pi^-\,\pi^0$	$B^+ + B^-$	<0.09	<0.025
	$A_1^+ + A_1^-$	<0.05	<0.04
	$A_2^+ + A_2^-$	<0.04	<0.02
	A_1^0	<0.06	<0.03
	A_2^0	<0.05	<0.01
	f^0	<0.02	<0.001
$n\,4\pi^+\,2\pi^-$	f^0	<0.015	...

[a]Ref. 20.

5. *Comparison with Other Energies*

In Table VIII are presented the production rates and the cross sections (corrected for unseen decay modes) of mesonic resonances observed in channels A, B, and C.

It has been reported[26] that at 8.5 GeV/c in channel A the percentage of ρ^0 production is (51.2 ±5.1)% and two ρ^0's are produced in (5.1 ±0.7)% of events. In channel B (45.1 ±6.8)% of the ω^0 and (3.7 ±1.3)% of the η production were found in the same experiment.

Our cross sections are compared in Table VIII with the values obtained at lower energies: 4 GeV/c (Ref. 18) and 5 GeV/c (Ref. 20). The cross sections are the same within errors at 5 and 8 GeV/c except for ρ^0 meson in channel B not observed at 5 GeV/c ($\sigma < 0.03$ mb) and copiously produced at 8 GeV/c ($\sigma = 0.32 \pm 0.05$ mb).

We note the equality of the ρ^0 and ω^0 production cross sections in the reactions $\pi + p \to p\pi^+\pi^+\pi^-(\rho^0$ or $\omega^0)$, which may be expected in the statistical model, since the mass, spin, and SU_3 multiplet assignment are the same for both resonances.

6. *Other Resonances*

In this section we give upper limits of production cross sections for other resonances.

In Fig. 20 the $\pi^\pm\pi^+\pi^-$ effective-mass distributions are presented for reactions A and B for all combi-

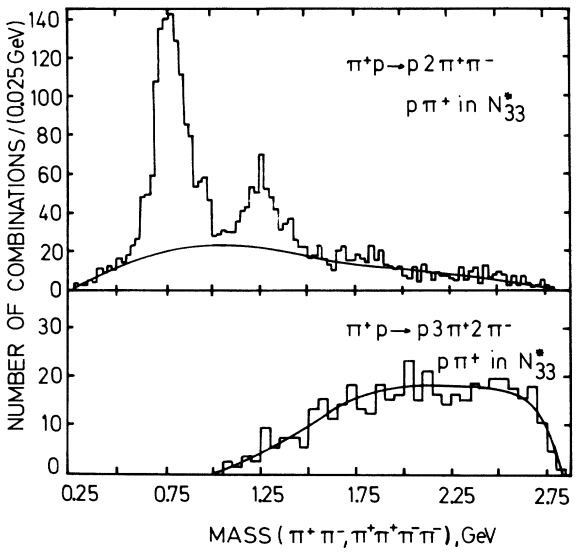

FIG. 22. Effective-mass distributions of the $\pi^+\pi^-$ system from the reaction $\pi^+p \to p\pi^+\pi^+\pi^-$ at 8 GeV/c taken from Ref. 36, and of the $\pi^+\pi^+\pi^-\pi^-$ system from channel A. Both distributions were obtained under the condition that the masses of the remaining π^+ and p fall in the N_{33}^{*++} band. Curves are drawn by hand.

nations and also for those which fulfill the condition that at least one $\pi^+\pi^-$ pair falls in the ρ band $[0.65 < M(\pi^+\pi^-) < 0.85$ GeV$]$. Upper limits of production cross sections in channel A and B are estimated to be 0.03 mb and 0.05 mb for the charged A_1 meson, and 0.03 mb and 0.04 mb for the charged A_2.

The upper limits of A_1^0 and A_2^0 production cross sections in channel B are estimated from the histogram shown in Fig. 17 to be 0.06 mb and 0.05 mb, respectively. In Fig. 21 the effective mass of the $\pi^+\pi^+\pi^-\pi^0$ system is plotted. In the lower histogram at least one $\pi^+\pi^-\pi^0$ combination was required to fall into the ω-mass region $[0.75 < M(\pi^+\pi^-\pi^0) < 0.825$ GeV$]$. The estimated upper limit for B meson production is 0.09 mb.

The upper limits of the cross sections for f^0 production in channels A, B, and C were calculated from the $\pi^+\pi^-$ mass distribution shown in Fig. 15 and are equal to 0.02 mb, 0.02 mb, and 0.015 mb, respectively.

The results presented in this section, uncorrected for unseen decay modes, are collected in Table IX and compared with the data at 5 GeV/c.[20]

7. *Branching Ratio* $(f^0 \to 4\pi)/(f^0 \to 2\pi)$

The Illinois group has reported[49] an observation of the decay mode $f^0 \to \pi^+\pi^+\pi^-\pi^-$ with the branching ratio

$$R = \frac{f^0 \to \pi^+\pi^+\pi^-\pi^-}{f^0 \to 2\pi} = 6.7\%.$$

Previous estimates of R lead to an upper limit of 4%.[44]

We estimated this branching ratio from the reaction $\pi^+ p \to N_{33}^{*++} f^0$ at 8 GeV/c. Figure 22 shows the mass distributions of the $\pi^+\pi^-$ system from the reaction $\pi^+ p \to p\pi^+\pi^+\pi^-$ measured by the Aachen-Berlin-CERN Collaboration,[36] and of the $\pi^+\pi^+\pi^-\pi^-$ system from channel A, both produced together with N_{33}^{*++}.

Using hand-drawn background curves, we estimate the number of f^0 decays in the mass region from 1.15 to 1.35 GeV to be 229 ±20 for the $\pi^+\pi^-$ decay mode and 3^{+6}_{-3} for the $\pi^+\pi^+\pi^-\pi^-$ mode, where both the fluctuation in numbers of events and the uncertainty of the background curves contribute to the errors. After correcting for a different amount of film measured in each experiment and for the decay mode $f^0 \to \pi^0\pi^0$, we obtain the value of the branching ratio

$$R = (2.2^{+4.5}_{-2.2})\%.$$

C. Production and Decay of ρ^0 and ω Mesons

1. *Distributions of Production Angle*

Distributions of the c.m. production angle were calculated for the ρ^0 in channels A and B and for the ω in channel B.

We considered the production angles θ of the $\pi^+\pi^-$ combinations in the ρ region (0.65–0.85 GeV) and in two control regions: 0.55–0.65 GeV and 0.85–0.95 GeV. For the ω meson the regions were defined as follows: 0.675–0.750 GeV, 0.750–0.825 GeV, and 0.825–0.900 GeV. The numbers of resonance and background combinations in each of the three regions were known from the fit (Secs. IV B 1 and IV B 2). By suitable normalization

TABLE X. Cross sections for $N^*(1236)$ production. Errors correspond to 68% confidence level.

Channel	Decay mode	This experiment m_0 (GeV)	This experiment $\Gamma(m_0)$ (GeV)	This experiment No events	This experiment σ (mb)	4 GeV/c[a] σ (mb)	5 GeV/c σ (mb)
A	$p\pi^+$	1.211 ± 0.009	0.100 ± 0.009	199 ± 43	0.158 ± 0.034[c]	0.204 ± 0.038	0.25 ± 0.05
	$p\pi^-$	fixed	fixed	58 ± 22	0.046 ± 0.018	···	<0.02[d]
B	$p\pi^+$	1.221 ± 0.006	0.098 ± 0.020	423 ± 72	0.330 ± 0.056[e]	0.197 ± 0.035	0.35 ± 0.05
	$p\pi^-$	fixed	fixed	58 ± 36	0.045 ± 0.028	···	<0.02[d]
	$p\pi^0$	fixed	fixed	33 ± 25	0.026 ± 0.020	···	<0.03[d]
C	$n\pi^-$	fixed	fixed	225 ± 42	0.175 ± 0.033	···	0.066 ± 0.030
	$n\pi^+$	fixed	fixed	0 ± 21	<0.016	···	···

[a]Ref. 18.
[b]Ref. 20.
[c]At 8.5 GeV/c (52.5 ± 6.5)% of N^{*++} production was reported in Ref. 26; the corresponding cross section is 0.234 ± 0.029 mb.
[d]Upper limits are given with 95% confidence level.
[e]At 8.5 GeV/c (44.0 ± 13.6)% of N^{*++} production was reported in Ref. 26; the corresponding cross section is 0.283 ± 0.088 mb.

and subtraction, the angular distributions of resonance combinations and of background combinations were separated. They are presented in Fig. 23 in which the background histograms (dashed) are normalized to the number of resonance combinations in the region of $\cos\theta < 0.7$.

A pronounced forward peak is observed in the ρ^0 and ω angular distributions whereas the anistropy is much smaller for the background combinations. The strongest effect is observed for the ρ^0 in channel A, where half of the resonant events are emitted in the forward direction ($0.7 < \cos\theta < 1.0$). A small backward peak of the ρ^0 in channel A can also be noted.

2. *Distributions of the Decay Angle*

Some spin alignment of the ρ^0 in channel A and of the ω in channel B has been reported at 5 GeV/c.[20] The effect has been observed in the decay angular distributions in the resonance rest frame when calculated with respect to the resonance momentum direction in the case of the ρ^0 and with respect to the transformed incident π^+ momentum in the case of the ω.

In order to see whether these effects would appear at our energy we performed similar calculations for the ρ^0 mesons in channel A and B using the helicity frame, and for the ω meson from channel B using the Jackson frame, as in Ref. 20.

In Figs. 24(a) and 24(b) we present angular distributions of the ρ^0-meson decay calculated for the

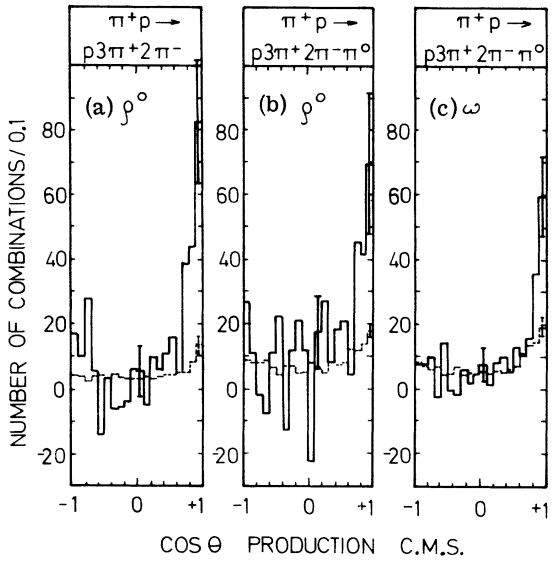

FIG. 23. Distributions of the c.m. production angles: (a) and (b) of ρ^0 in channels A and B; (c) of ω in channel B. Subtracted background estimated from the adjacent regions is shown by dashed histograms.

$\pi^+\pi^-$ combinations in the mass region 0.65–0.85 GeV from which background obtained from the adjacent regions of 0.45–0.65 GeV and 0.85–1.05 GeV was subtracted. No significant deviation from isotropy is observed. In channel A the $\cos\theta$ distribution [Fig. 24(a)] may be described by the formula

$$W(\cos\theta) = N(1 + c\cos^2\theta),$$

with $c = -0.85 \pm 0.67$, where N is a normalization constant. The constant c was also consistent with zero in Ref. 20. However, with an additional cut on the transfer u from the initial proton to the ρ^0 the authors of Ref. 20 have obtained a positive value of c.

The ω band was defined as 0.75–0.85 GeV and adjacent regions 0.10-GeV wide were used to estimate the background to be subtracted. The resulting $\cos\theta$ distribution for the ω-meson decay [shown in Fig. 24(c)] is described by the formula given above, with the constant c equal to $+2.0 \pm 1.2$. This observation is similar to that reported in Ref. 20.

V. BARYON RESONANCES

A. Cross Sections for $N^*_{33}(1236)$ Production

The effective-mass distributions of the nucleon-$\pi^\pm$ systems for the fitted channels are shown in Figs. 25–27. A strong production of N^{*++}_{33} is observed in channels A and B [Figs. 25(b) and 26(b)] and a considerable signal of N^{*-}_{33} in channel C [Fig. 27(b)]. All the mass distributions of the nucleon-pion system were fitted with the Breit-Wigner formula[50] and the modified phase-space background which included reflections of the ρ^0 in channel A and of the ρ^0, ω production in channel B. In

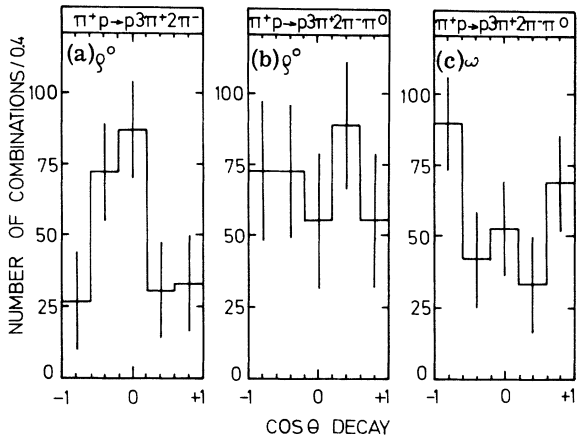

FIG. 24. Distribution of the decay angle: (a) and (b) of the ρ^0 in channels A and B, respectively, calculated in the helicity frame; (c) of the ω in channel B, calculated in the Jackson frame.

TABLE XI. Upper limits of cross sections for production of $N^*(1518)$ and $N^*(1688)$, estimated with 68% confidence level.

Reaction $\pi^+p \to$	Channel	N^* decay mode	$N^*(1518)$ σ (μb)	$N^*(1688)$ σ (μb)
$N^{*0}3\pi^+\pi^-$	A	$p\pi^-$	<72	<88
	B	$p\pi^-\pi^0$		
	C	$n\pi^+\pi^-$		
$N^{*0}3\pi^+\pi^-\pi^0$	B	$p\pi^-$	<14	<24
$N^{*0}3\pi^+\pi^-m\pi^0$	D	$p\pi^-$	<44	<28
$N^{*+}3\pi^+2\pi^-$	B	$p\pi^0$	<56	<56
	C	$n\pi^+$		
$N^{*+}2\pi^+\pi^-$	A	$p\pi^+\pi^-$	<37	<35
$N^{*+}2\pi^+\pi^-\pi^0$	B	$p\pi^+\pi^-$	<58	<82
$N^{*+}2\pi^+\pi^-m\pi^0$	D	$p\pi^+\pi^-$	<110	<120

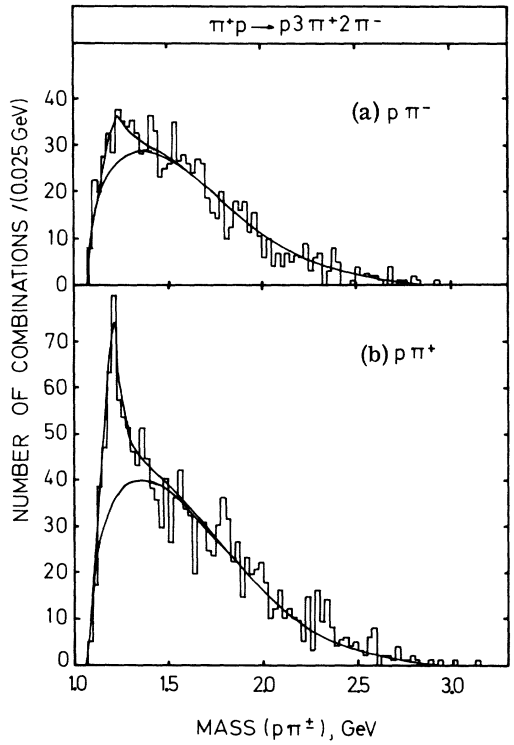

FIG. 25. Effective-mass distributions of the $p\pi^-$ and $p\pi^+$ systems for channel A. The upper solid lines show the results of the fits with a sum of the Breit-Wigner distribution and the modified phase-space background shown below.

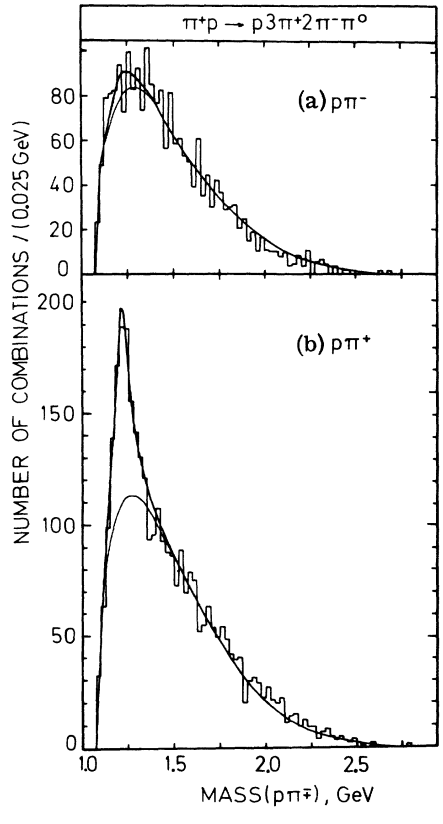

FIG. 26. Effective-mass distributions of the $p\pi^-$ and $p\pi^+$ systems for channel B. The upper solid lines are the results of the fits with a sum of the Breit-Wigner distribution and the modified phase-space background shown below.

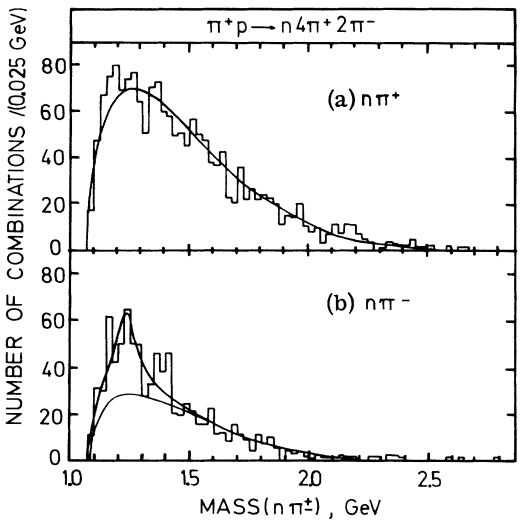

FIG. 27. Effective-mass distributions: (a) of the $n\pi^+$ system, (b) of the $n\pi^-$ system in channel C. Solid line in (a) shows the prediction of the relativistic phase space. The upper solid line in (b) shows the result of the fit with a sum of the Breit-Wigner curve and the phase-space curve shown below.

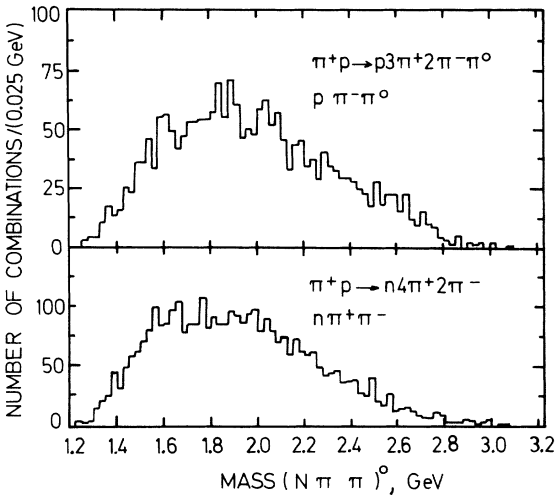

FIG. 29. Effective-mass distributions of the $p\pi^-\pi^0$ system in channel B and of the $n\pi^+\pi^-$ system in channel C.

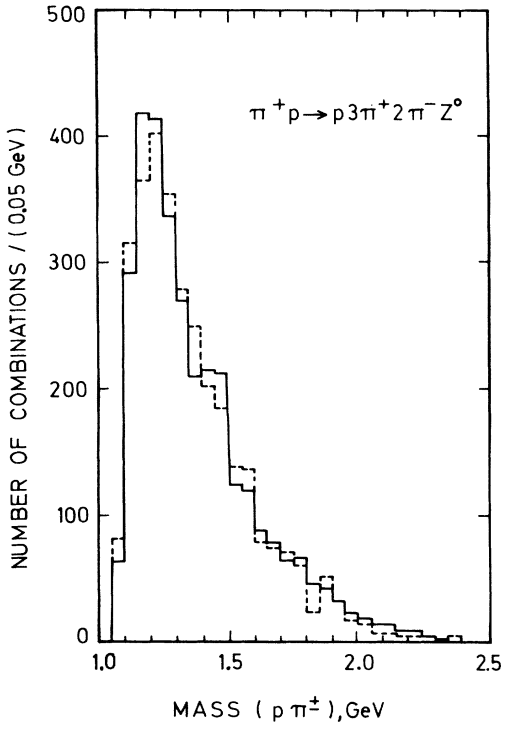

FIG. 28. Effective-mass distributions of the $p\pi^+$ system (solid histogram) and of the $p\pi^-$ system (dashed histogram) in channel D. The $p\pi^-$ mass distribution is normalized to the area of the $p\pi^+$ histogram.

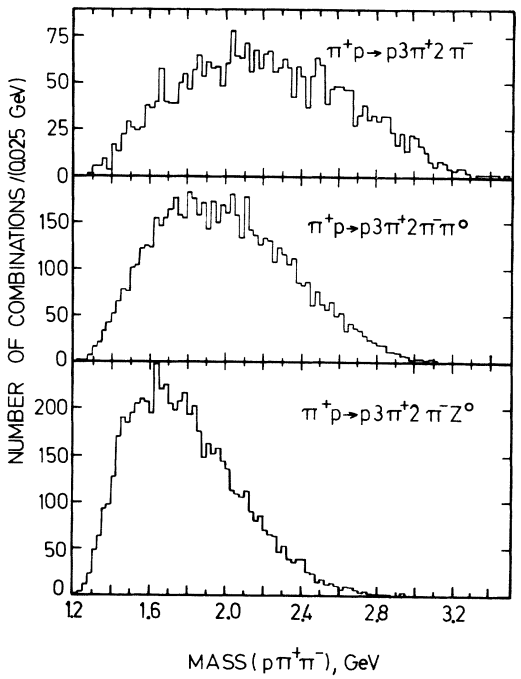

FIG. 30. Effective-mass distributions of the $p\pi^+\pi^-$ system in channels A, B, and D.

channel C the modified phase space is practically identical with the ordinary phase space.

In Table X are presented the fitted values of mass, width, and production cross section of $N^*_{33}(1236)$ obtained in this experiment and compared with available data at other energies. In channels A and B, where significant N^{*++}_{33} production is observed, the mass and width of N^{*++}_{33} were fitted. In other cases the values $m_0 = 1230$ MeV, $\Gamma(m_0) = 120$ MeV were fixed.

For channel D the $p\pi^+$ mass distribution solid histogram and the $p\pi^-$ mass distribution normalized to the same area (dashed histogram) are shown in Fig. 28. No N^*_{33} production is observed.

B. Search for Other Resonances

Apart from $N^*_{33}(1236)$ no other structures are observed either in $N\pi$ or in $N\pi\pi$ mass distributions, shown in Fig. 29 ($I_3 = -\frac{1}{2}$) and Fig. 30 ($I_3 = +\frac{1}{2}$).

The $N^*(1585)$ and $N^*(1688)$ resonances were observed in production experiments.[51] We estimated upper limits for their production cross sections in the following reactions:

for N^* in $I_3 = -\frac{1}{2}$ state,

$\pi^+ p \to N^{*0} 3\pi^+\pi^-$

$N^{*0} 3\pi^+\pi^-\pi^0$

$N^{*0} 3\pi^+\pi^- m\pi^0, \quad m > 1$

for N^* in $I_3 = +\frac{1}{2}$ state,

$\pi^+ p \to N^{*+} 3\pi^+ 2\pi^-$

$N^{*+} 2\pi^+\pi^-$

$N^{*+} 2\pi^+\pi^-\pi^0$

$N^{*+} 2\pi^+\pi^- m\pi^0, \quad m > 1.$

In Table XI we present upper limits for the production cross sections estimated in our experiment (not corrected for unseen decay modes).

The energy dependence of the cross section for the reaction $\pi^+ p \to p 2\pi^+\pi^-$ shows a bump at about 2.9-GeV c.m. energy. It can be considered as a reflection of the formation of the $N^*(2850)$ isobar and its subsequent decay into $p\pi^+\pi^+\pi^-$.

A preliminary analysis[32] based on $\frac{1}{5}$ of the present statistics seemed to show that the $N^*(2850)$ isobar was produced in reaction B. The peak was observed in the $p\pi^+\pi^+\pi^-$ mass distribution in the region 2.8–2.9 GeV and corresponded to the cross section of 155 ± 52 μb.

Figure 31 shows the $p\pi^+\pi^+\pi^-$ mass distribution for full statistics. The solid line is calculated from the modified-phase-space model. There is no evidence for the $N^*(2850)$ production. The estimated cross section is equal to $0 \pm {}^{17}_{0}$ μb.

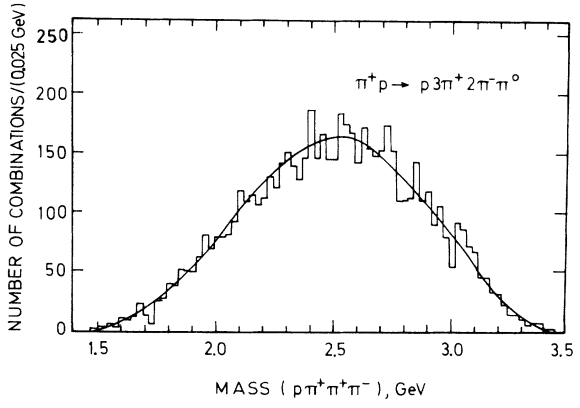

FIG. 31. Effective-mass distribution of the $p\pi^+\pi^+\pi^-$ system in channel B. Solid line shows the prediction of the modified phase-space model.

C. Properties of N^{*++}_{33} Production

The distributions of the four-momentum transfer from the incident proton to the $p\pi^+$ system calculated for N^*_{33} mass band are shown in Figs. 32(a) and 32(b) for channels A and B, respectively. The corresponding distributions for the $p\pi^-$ system are presented in these figures as shaded histograms. Figures 32(c) and 32(d) show the t distributions of the N^{*++}_{33} for channels A and B. They represent the difference between the experimental distribution of the $p\pi^+$ system and the t distribution for the $p\pi^-$ system normalized to the number of nonresonant combinations in the N^{*++}_{33} band. Solid lines in Figs. 32(c) and 32(d) show the distributions of t to the secondary proton smoothed out by using the $F(t)$ model and normalized to the total number of N^{*++}_{33}. In both channels, the t distributions of N^{*++}_{33} are sharper than those of protons. As it is seen, more than 50% of N^{*++}_{33} is produced with t less than 1 GeV^2 and, practically, there is no N^{*++}_{33} produced with t greater than 3 GeV^2.

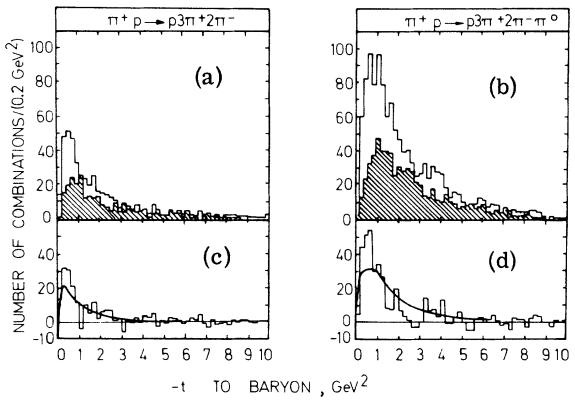

FIG. 32. Distributions of the squared four-momentum transfer, t, from the initial proton to the $p\pi$ systems in the N^*_{33} band: (a) for reaction A; (b) for reaction B. Upper histograms correspond to the $p\pi^+$ systems and hatched histograms to the $p\pi^-$ systems. The resulting distributions of t to N^{*++}_{33} are shown in (c) and (d) and compared with the distributions of t to secondary proton, smoothed out by the $F(t)$ function (solid curves).

Figure 33 shows the $\cos\theta$ distribution of the N_{33}^{*++} decay angle, calculated with respect to the axis parallel to the N_{33}^{*++} momentum vector transformed to its rest frame. We used as a background the $\cos\theta$ distribution of the $p\pi^-$ system in the corresponding mass band. The distribution of $\cos\theta$ for channel A is consistent with the formula $W(\cos\theta) = N(1 + c\cos\theta)$, where N is a normalization constant and $c = 0.57 \pm 0.34$. The data do not require the $\cos^2\theta$ term. The distribution of $\cos\theta$ is isotropic in channel B. There is no significant deviation from isotropy in the distribution of azimuthal decay angle.

We can conclude that no alignment of N_{33}^{*++} spin is observed. The term proportional to $\cos\theta$ for channel A, if present, can be explained by an interference between the P wave and the background S wave.

VI. ASSOCIATED PRODUCTION OF RESONANCES

A. The Reaction $\pi^+ p \to N_{33}^{*++} X^0$

The Dalitz plot for ten events of the reaction $\pi^+ p \to p\pi^+ X^0$ is shown in Fig. 34. There is a distinct group of five events in which the $p\pi^+$ mass falls in the $N^*(1236)$ region, 1.5–1.35 GeV. Assuming[52] that all these events represent the two-body reaction $\pi^+ p \to N^{*++} X^0$ we have calculated the cross section

$$\sigma(\pi^+ p \to N^{*++} X^0) = 30 \pm 13 \ \mu\text{b}$$

corrected for unseen decay modes of the X^0 meson.[45] This value of the cross section is compared in Fig. 35 with the data at lower energies.[18,20,53] In the same figure the cross sections for the reaction $\pi^+ p \to N^{*++} \eta$ are plotted.[54]

The slope A in the formula which describes the differential cross section for the reaction $N^{*++} X^0$,

$$\frac{d\sigma}{dt} = C e^{At'}, \quad t' = t - t_{\min},$$

has been determined with the use of the maximum-likelihood method of Bartlett.[55] We have found $A = 4.5 \pm 2.1$ GeV^{-2} for our events and $A = 2.8 \pm 1.0$ GeV^{-2} for the events reported at 5 GeV/c.[20] The value for the combined sample of events at 5 and 8 GeV/c is $A = 3.3 \pm 1.0$ GeV^{-2}.

By comparing the $N^{*++} X^0$ and $N^{*++}\eta^0$ cross sections at 8 GeV/c, we have determined the η^0-X^0 mixing angle defined by

$$|X^0\rangle = |\eta_1\rangle \cos\theta + |\eta_8\rangle \sin\theta,$$

$$|\eta^0\rangle = -|\eta_1\rangle \sin\theta + |\eta_8\rangle \cos\theta.$$

Within the framework of the quark model one may prove the following relation[56]:

$$\frac{\bar{\sigma}(\pi^+ p \to N^{*++}\eta^0)}{\bar{\sigma}(\pi^+ p \to N^{*++} X^0)} = \rho,$$

where $\bar{\sigma}$ is the transition-matrix element squared and

$$\pm\sqrt{\rho} = \tan(\theta_0 - \theta), \quad \theta_0 = \arctan(\tfrac{1}{2})^{1/2}.$$

As is well known, there is no unique prescription for accounting for the mass differences in the quark model. We have tried two methods. In the first one we have used the cross sections σ at the

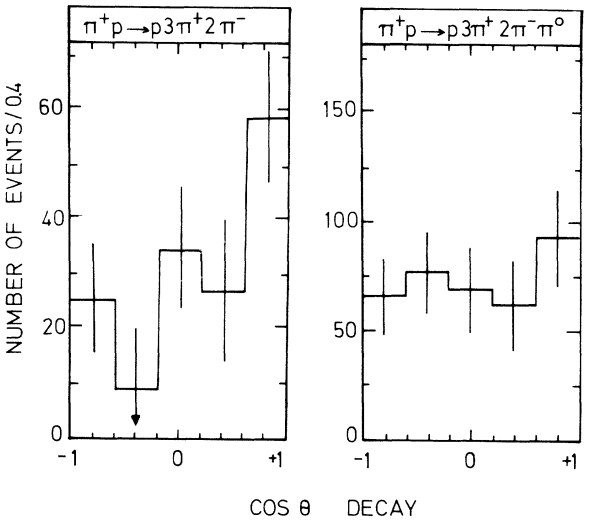

FIG. 33. Distributions of the decay angle of N_{33}^{*++} for channels A and B.

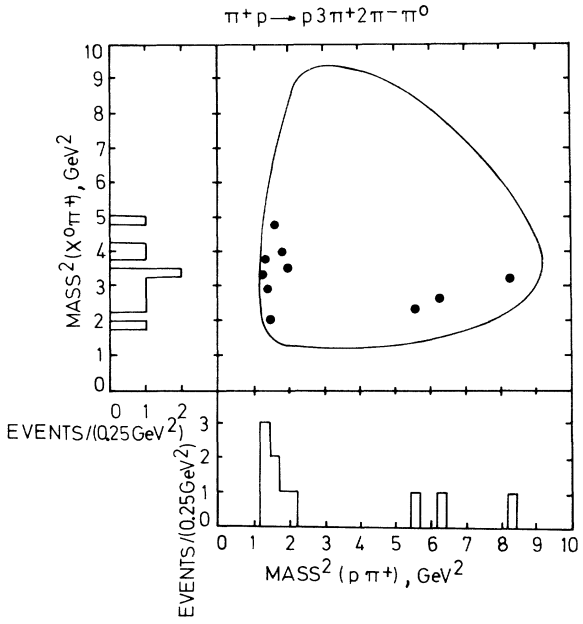

FIG. 34. Dalitz plot for 10 events of the reaction $\pi^+ p \to p\pi^+ X^0$.

same Q value, corrected for different phase space available according to the formula

$$\bar{\sigma} = s\frac{p_{in}}{p_{out}}\sigma,$$

where s is the c.m. energy squared and p_{in}, p_{out} are the c.m. momenta before and after collision. In this method the cross section for the reaction $\pi^+p \to N^{*++}X^0$ at 8 GeV/c should be compared with the $N^{*++}\eta$ cross section at 6.4 GeV/c. We obtained for it the value of 43 μb by interpolating the existing data[54] with the formula $\sigma \sim p_{lab}^{-n}$. The comparison of this value with $\sigma = 30 \pm 13$ μb for $N^{*++}X^0$ production at 8 GeV/c gives

$$\rho = 1.1 \pm 0.4,$$
$$\theta(+\sqrt{\rho}) = -11° \pm 6°,$$
$$\theta(-\sqrt{\rho}) = -98° \pm 6°.$$

In the second attempt we have used the data for $N^{*++}X^0$ and $N^{*++}\eta$ (Ref. 36) production at 8 GeV/c only. The cross sections were corrected only for the difference in t_{min} (0.06 GeV^2 for X^0, 0.01 GeV^2 for η production) taking the value of the slope of the differential cross section $A = 3.3$ GeV^{-2} for the X^0 and $A = 0$ in the small-t region for reaction $\pi^+p \to N^{*++}\eta$.[36] Corrections calculated in this way are 20% for the X^0 and 2.5% for the η^0. The results

$$\rho = 1.4 \pm 0.7,$$
$$\theta(+\sqrt{\rho}) = -15° \pm 7°,$$
$$\theta(-\sqrt{\rho}) = -95° \pm 7°,$$

are not very different from those obtained in the first method.

Both discussed values of the η^0-X^0 mixing angle $\theta(+\sqrt{\rho})$ agree well with the value $\theta = \pm 10.4°$ determined from the quadratic mass formula for the 0^- nonet.[44]

Recently the LRL group[57] made a very accurate determination of the η^0-X^0 mixing angle. Their results are:

$$\theta(+\sqrt{\rho}) = -29.0° \pm 3.3°,$$
$$\theta(-\sqrt{\rho}) = -80.4° \pm 3.3°.$$

B. The Reaction $\pi^+p \to N_{33}^{*++}D^0$

We have searched for the two-body reaction $\pi^+p \to N^{*++}(1236)D^0$. Figure 36(a) shows the effective-mass distribution of the $p\pi^+$ system produced together with the $\pi^+\pi^+\pi^-\pi^-\pi^0$ combinations having the mass in the D^0 band and containing at least one $\pi^+\pi^-\pi^0$ combination in the η band. The curve shows the prediction of the modified phase space normalized to the experimental histogram above 1.5 GeV.

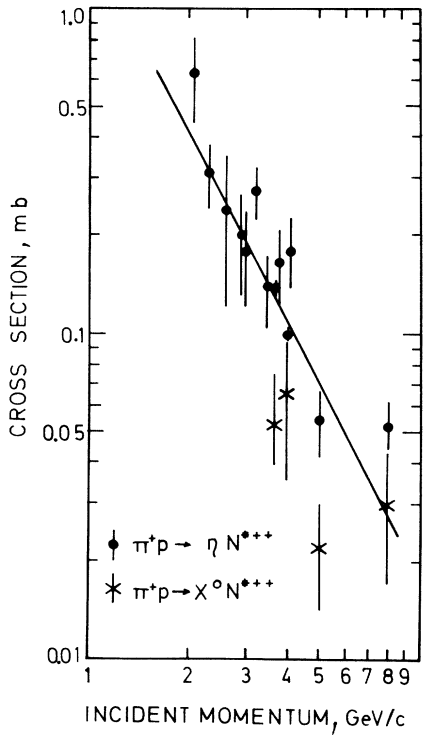

FIG. 35. Cross section for the reaction $\pi^+p \to N^{*++}\eta^0$ and $\pi^+p \to N^{*++}X^0$ as a function of incident laboratory momentum.

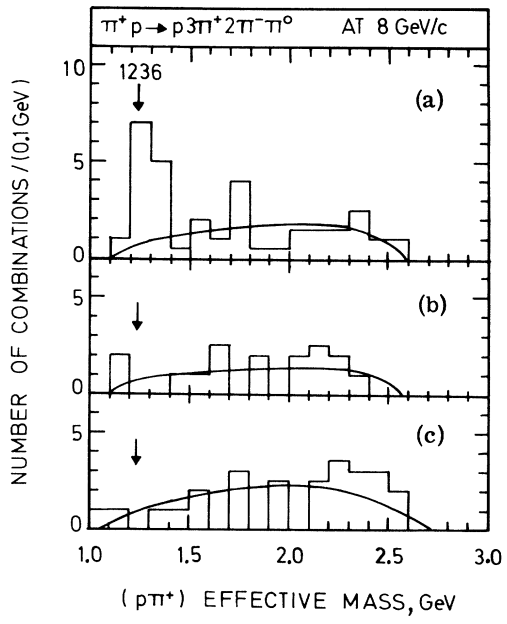

FIG. 36. The effective-mass distributions of the $p\pi^+$ system: (a) associated with the D^0 events, (b) and (c) associated with the control $\pi^+\pi^+\pi^-\pi^-\pi^0$ combinations (see text). The curves are calculated from the modified phase-space model.

An excess of 8 ± 3 events is present at the position of the $N^*(1236)$.

We have also studied the $p\pi^+$ mass distribution using the following control conditions for the remaining $\pi^+\pi^+\pi^-\pi^-\pi^0$ system:

(1) The $\pi^+\pi^+\pi^-\pi^-\pi^0$ system had the mass in the D^0 band and contains no "η" but at least one $\pi^+\pi^-\pi^0$ combination in the mass region 0.6–0.7 GeV, adjacent to η.

(2) The $\pi^+\pi^+\pi^-\pi^-\pi^0$ system contains "η" and has the mass in the region 1.175–1.275 GeV or 1.375–1.475 GeV, adjacent to D^0.

The $p\pi^+$ mass distributions obtained under these two conditions, plotted in Figs. 36(b) and 36(c), agree with the modified phase-space curves and show no enhancement at the $N^*(1236)$ mass. Therefore we may interpret the excess in Fig. 36(a) as due to the two-body final state $N^{*++}(1236)D^0$. The estimated cross section for the reaction

$$\pi^+ p \to N^{*++}(1236)D^0$$
$$\to N^{*++}(1236)\eta\pi^+\pi^-$$
$$\to p\pi^+\pi^+\pi^+\pi^-\pi^-\pi^0$$

is 6 ± 2 μb.

C. Search for Two-Body Reactions $\pi^+ p \to p +$ Meson

We looked for the evidence of the two-body reactions $\pi^+ p \to p +$ meson in channels A and B. We studied the effective-mass distributions of 5π and 6π systems without restrictions and also applying cuts on squared four-momentum transfer t or requiring the ρ^0, ω, η, or X^0 to be present within the pionic system. No significant peaking was observed.

In particular, all the $X^0\pi^+$ combinations have mass squared larger than 1.9 GeV, as can be seen in Fig. 34. The upper limit, corresponding to one event, for the cross section for the reaction $\pi^+ p \to pM^+ \to pX^0\pi^+$, where M^+ is a mesonic resonance (e.g., A_1, A_2) is therefore equal to 6 μb, after correcting[45] for unseen decay modes of X^0. Using the cross sections[36] for the reactions $\pi^+ p \to pA_1^+$ and $\pi^+ p \to pA_2^+$ at 8 GeV/c, we estimate the upper limit for the branching ratio $[A^+ \to X^0\pi^+]/[A^+ \to \text{(all modes)}]$ to be 2.5% for the A_1 and A_2 mesons.

D. Associated Production of N_{33}^{*++}, ρ^0, and ω

1. *Determination of Cross Sections*

It has been shown in Secs. IV B and V A that the following resonances are copiously produced: in channel A the $N^{*++}(1236)$ (in 39% of events) and ρ^0 (66%), in channel B the N^{*++} (39%), ρ^0 (38%), and ω (31%). Consequently, on the average, slightly more than one resonance combination per event is present in each of the channels.

In this section we present a method of determination of the cross sections for simultaneous production of these resonances. We assume that the events of channel A are an incoherent mixture of the six reactions listed in Table XII. In channel B eight reactions listed in Table XIII were considered. Weakly produced resonances and simultaneous production of two ρ^0 mesons in channel B were neglected. The X^0 events were removed from the experimental sample.

The analysis was performed in the three-dimensional space of the effective masses of the systems: $\pi_1^+\pi_1^-$, $\pi_2^+\pi_2^-$, and $p\pi_3^+$ in channel A and $\pi_1^+\pi_1^-$, $\pi_2^+\pi_2^-\pi^0$, and $p\pi_3^+$ in channel B. The method is very similar in the two channels and is outlined below

TABLE XII. Results of the three-dimensional fit for channel A. The frequencies in the last column are calculated assuming "independent production" of resonances.

	Reaction	Number of events	Cross section σ (μb)	Frequency (%)	"Independent production" (%)
$A1$	$N^{*++}\rho^0\rho^0$	53 ± 27	42 ± 22	10.5 ± 5.4	4.3
$A2$	$p\rho^0\rho^0\pi^+$	14 ± 44	11 ± 35	2.8 ± 8.7	10.8
$A3$	$N^{*++}\rho^0\pi^+\pi^-$	83 ± 59	66 ± 47	16.5 ± 11.7	13.7
$A4$	$p\rho^0\pi^+\pi^+\pi^-$	98 ± 94	78 ± 75	19.4 ± 18.6	33.8
$A5$	$N^{*++}\pi^+\pi^+\pi^-\pi^-$	9 ± 45	7 ± 36	1.8 ± 8.9	10.8
$A6$	$p\pi^+\pi^+\pi^+\pi^-\pi^-$	247 ± 61	196 ± 49	49.0 ± 12.1	26.6
$A1+A3$	N^{*++} and at least one ρ^0	136 ± 45	108 ± 36	27.0 ± 8.9	18.0
$A1+A2$	$\rho^0\rho^0$ (with or without N^{*++})	67 ± 40	53 ± 32	13.3 ± 7.9	15.1
$A1+A2+A3$	at least two resonances in an event	150 ± 68	119 ± 54	29.8 ± 13.5	28.8

for channel B only.

Every measured event contributes 12 points in the defined three-dimensional space of $M_1 = M(\pi_1^+ \pi_1^-)$, $M_2 = M(\pi_2^+ \pi_2^- \pi^0)$, and $M_3 = M(p\pi_3^+)$. The data were grouped in bins containing at least ten entries each.

We have assumed that each of the considered reactions can be described by the modified phase space and the Breit-Wigner formulas for resonances. This assumption leads to a very good agreement with one-dimensional mass distributions. A sample of Monte Carlo events was generated according to the modified phase space. Their density is denoted by $\Delta_{MPS}(M_1, M_2, M_3)$. The predicted density, e.g., for reaction $B5$ is

$$D_5(M_1, M_2, M_3) = \Delta_{MPS}(M_1, M_2, M_3) f_{BW}(M_1) f_{BW}(M_3),$$

where $f_{BW}(M_1)$ is the Breit-Wigner factor for the ρ^0, and $f_{BW}(M_3)$ that for the $N^{*++}(1236)$. For every reaction the density $D_i(M_1, M_2, M_3)$ was computed by weighting the generated events with the appropriate Breit-Wigner formulas. Each generated event gives 12 points in the three-dimensional space and all these points get the same weight calculated for one, arbitrarily chosen, set of indices. Due to this procedure reflections of resonances are automatically included.

The calculated density for each reaction was normalized to the value of 12. The total density is

$$D(M_1, M_2, M_3) = \sum_{i=1}^{8} N_i D_i(M_1, M_2, M_3),$$

where the coefficient N_i is the number of events of the ith reaction. The values of N_i were determined from a fit of the above expression $D(M_1, M_2, M_3)$ to the experimental distribution by the χ^2 method. In the fit, the sum $\sum_{i=1}^{8} N_i$ was constrained to be equal to the number of events in the experimental sample. The numbers of events obtained are given in Tables XII and XIII, together with the corresponding percentages and the cross sections, corrected for unseen decay modes.

The value of χ^2 is 150 for 107 degrees of freedom in channel A and $\chi^2 = 227$ for 137 degrees of freedom in channel B. Taking into account the rough character of the modified-phase-space model and the fact that the production of some resonances was neglected, the fits obtained may be considered as satisfactory.

We have checked that the numbers of resonance combinations of N^{*++}, ω, and ρ^0, resulting from the three-dimensional fits, agree well with the numbers obtained previously by the one-dimensional mass fitting.

2. *Discussion of Results*

The most prominent feature of the results obtained is a high percentage of events without any resonance production: about 50% in channel A and 30% in channel B. However, it should be noted that resonances which were neglected in the analysis may contribute more events to this reaction than to the others.

The three-body reaction $N^{*++}\rho^0\rho^0$ is found to be produced in $(10.5 \pm 5.4)\%$ of events of channel A. Because of a large error the evidence is not conclusive. The reaction $N^{*++}\rho^0\omega$ is detected with the

TABLE XIII. Results of the three-dimensional fit for channel B. The cross sections are corrected for unseen decay modes. The frequencies in the last column are calculated assuming "independent production" of resonances.

	Reaction	Number of events	Cross section (μb)	Frequency (%)	"Independent production" (%)
$B1$	$N^{*++}\omega^0\rho^0$	75 ± 25	66 ± 22	7.0 ± 2.3	6.6
$B2$	$p\omega\rho^0\pi^+$	48 ± 38	41 ± 33	4.5 ± 3.5	8.2
$B3$	$N^{*++}\omega^0\pi^+\pi^-$	229 ± 44	199 ± 40	21.3 ± 4.1	9.6
$B4$	$p\omega^0\pi^+\pi^+\pi^-$	41 ± 50	36 ± 43	3.8 ± 4.6	12.0
$B5$	$N^{*++}\rho^0\pi^+\pi^-\pi^0$	128 ± 67	100 ± 53	11.9 ± 6.2	11.4
$B6$	$p\rho^0\pi^+\pi^+\pi^-\pi^0$	183 ± 73	143 ± 57	17.0 ± 6.8	14.2
$B7$	$N^{*++}\pi^+\pi^+\pi^-\pi^-\pi^0$	42 ± 77	33 ± 60	3.9 ± 7.2	16.6
$B8$	$p\pi^+\pi^+\pi^+\pi^-\pi^-\pi^0$	319 ± 88	250 ± 71	29.7 ± 8.2	20.5
$B1+B3$	$N^{*++}\omega^0$ (with or without ρ^0)	304 ± 35	265 ± 37	28.3 ± 3.3	16.3
$B1+B2$	$\omega^0\rho^0$ (with or without N^{*++})	123 ± 32	105 ± 29	11.5 ± 3.0	14.9
$B1+B5$	$N^{*++}\rho^0$ (with or without ω^0)	203 ± 68	166 ± 54	18.9 ± 6.3	18.0
$B1+B2+B3+B5$	at least two resonances in an event	480 ± 92	406 ± 87	44.6 ± 8.6	35.8

statistical significance of three standard deviations and occurs in $(7.0 \pm 2.3)\%$ of events of channel B.

In both channels the percentage of events with the N^{*++} but no other resonance is low. The same is true for the ω in channel B. Instead, the ω is frequently produced with the N^{*++}, namely in $(21.3 \pm 4.1)\%$ of events.

The percentage of most of the reactions are determined with large uncertainties, which are often strongly correlated, i.e., the off-diagonal terms of the error matrix are comparable to the diagonal terms. By grouping some reactions one can obtain more significant results. In channel A the percentage of events with N^{*++} and at least one ρ^0 is $(27.0 \pm 8.9)\%$, and with two ρ^0's (with or without N^{*++}) $(13.3 \pm 7.9)\%$. In channel B the N^{*++} and ω (with or without ρ^0) are produced together in $(28.3 \pm 3.3)\%$ of the events, N^{*++} together with ρ^0 in $(18.9 \pm 6.3)\%$, and ω together with ρ^0 in $(11.5 \pm 3.0)\%$.

In channel A in $(29.8 \pm 13.5)\%$ of events at least two resonances are produced simultaneously. In channel B the percentage of such events is $(44.6 \pm 8.6)\%$.

We have compared the determined frequencies of various reactions with the hypothesis that each resonance is produced independently of other resonances.

In channel A the probability p_{N^*} of producing the N^{*++} is equal to the ratio of the resonance N^{*++} combinations to the total number of events. Two ρ^0 mesons can be produced in one event and therefore we define the probability p_ρ as one half of the ρ^0 production rate. The probability of producing n ρ^0 mesons (where $n = 0, 1, 2$) is given by the binomial distribution

$$P(n) = \binom{2}{n} p_\rho{}^n (1 - p_\rho)^{2-n} .$$

By multiplying $P(n)$ by p_{N^*} one obtains the probability of simultaneous production of the N^{*++} and n ρ^0 mesons.

In channel B we neglect the possibility of producing two ρ^0 mesons in one event and we define the probabilities p_{N^*}, p_ρ, and p_ω as the production rates of N^{*++}, ρ^0, and ω, respectively. The expected frequencies of various reactions are calculated by multiplying the appropriate probabilities, e.g., $(1 - p_{N^*}) p_\rho p_\omega$ for the reaction $p\pi^+\rho^0\omega$. All the values of the production rates were taken from the three-dimensional fits.

The numbers obtained are given in the last columns of Tables XII and XIII. They agree with the experimentally determined frequencies within large errors. The only significant deviation is a more frequent associated production of N^{*++} and ω, which occurs in $(28.3 \pm 3.3)\%$ of events whereas the predicted percentage is 16.3%.

3. *Comparison with Other $\pi^+ p$ and $\pi^- p$ Experiments*

Associated production of resonances in six-prong $\pi^+ p$ experiments has been studied at 4 GeV/c,[18] 5 GeV/c,[20,22] and 8.5 GeV/c.[26]

At 4 GeV/c only channel B was considered. High production rates of N^{*++}, $(78 \pm 9)\%$, and of ω, $(62 \pm 4)\%$, imply a substantial amount of their associated production. A simultaneous fit to the mass distributions of $p\pi^+$ and $\pi^+\pi^-\pi^0$ with the phase-space predictions gave the cross sections, listed in Table XIV, for the four reactions studied. For comparison, our estimates at 8 GeV/c are also given. A striking increase of the cross section for the reaction without resonances is observed. In both experiments the associated production of N^{*++} and ω is much stronger than the production of the N^{*++} alone, and the cross section for the production of the ω without N^{*++} is consistent with zero.

In channel A in the 5-GeV/c experiment, the associated production of N^{*++} (produced in 60% of the events) and ρ^0 (63%) was studied. The two-dimensional distribution of the $p\pi^+$ and $\pi^+\pi^-$ effective masses was fitted with the phase-space predictions for four reactions: $p\pi^+\pi^+\pi^+\pi^-\pi^-$, $p\rho^0\pi^+\pi^+\pi^-$, $N^{*++}\pi^+\pi^+\pi^-\pi^-$, $N^{*++}\rho^0\pi^+\pi^-$. The reaction $N^{*++}\rho^0\pi^+\pi^-$ was estimated to take place in $(50 \pm 11)\%$ of events. This result is not directly comparable to our data, because it neglects the possibility of the production of two ρ^0's in one event.

The associated production of N^{*++} and ω at 5 GeV/c was reported to occur in about 27% of events of channel B.

At 8.5 GeV/c the simultaneous production of two ρ^0 mesons in channel A was studied by the mass-strip method. The percentage of such an event was reported to be $(5.1 \pm 0.7)\%$ with surprisingly small error. Our estimate at 8 GeV/c is $(13.3 \pm 7.9)\%$, based on comparable statistics.

For completeness we have also collected the

TABLE XIV. Cross sections, corrected for unseen decay modes, for the production of N^{*++} and ω in channel B. The cross sections at 8 GeV/c were calculated from the data of Table XIII neglecting the fact that some of $\pi^+\pi^-$ combinations form the ρ^0.

Reaction	Cross section (μb) 4 GeV/c[a]	8 GeV/c
$N^{*++}\omega\pi^+\pi^-$	150 ± 33	265 ± 37
$N^{*++}\pi^+\pi^+\pi^-\pi^-\pi^0$	58 ± 13	133 ± 31
$p\omega\pi^+\pi^+\pi^-$	28 ± 28	77 ± 33
$p\pi^+\pi^+\pi^+\pi^-\pi^-\pi^0$	0 ± 13	393 ± 44

[a]Ref. 18.

available data on associated production of resonances in $\pi^- p$ interactions in the six-body channel $p\pi^+\pi^+\pi^-\pi^-\pi^-$ and the seven-body channel $p\pi^+\pi^+\pi^-\pi^-\pi^-\pi^0$. Results were reported at 3.9 GeV/c,[2] 6 GeV/c,[6,58] and 11 GeV/c.[14] In this region of incident π^- momentum the production of $N^{*++}(1236)$ and ρ^0 (or ω) is abundant and partly simultaneous, but in contrast with the corresponding $\pi^+ p$ channels, it cannot be accompanied by a third resonance, because the remaining system consists of two negative pions.

In the experiment at 3.9 GeV/c the events of the six-body channel were fitted by the maximum-likelihood method on the assumption of the phase-space model with incoherent resonance production. The following cross sections were obtained:

$$\pi^- p \to N^{*++}\pi^+\pi^-\pi^-\pi^-, \quad 40 \pm 6\ \mu\text{b},$$
$$p\rho^0\pi^+\pi^-\pi^-, \quad 3 \pm 9\ \mu\text{b},$$
$$pA_1^-\pi^+\pi^-, A_1^- \to \rho^0\pi^-, \quad 25 \pm 8\ \mu\text{b},$$
$$N^{*++}\rho^0\pi^-\pi^-, \quad 23 \pm 12\ \mu\text{b}.$$

The cross section for the reaction $N^{*++}\rho^0\pi^-\pi^-$ can be compared with the value $\sigma = 48 \pm 6$ μb at 6 GeV/c determined by the mass-strip technique with the phase-space background. At 11 GeV/c the cross section of 75 μb was reported.

The seven-body channel was investigated only in the experiment at 6 GeV/c and the obtained value of the cross section for the associated production of the N^{*++} and ω is 40 ± 8 μb, uncorrected for unseen ω decays.

More data of higher precision are needed to increase our knowledge of the associated production of resonances. The analysis is obscured by a large number of background combinations in multibody processes. A more serious difficulty comes from the fact that the hand-drawn curves so frequently used in the one-dimensional mass fitting are not applicable in the case of many-dimensional distributions. One needs, then, a model able to describe, quantitatively, various contributing reactions. The obtained results on associated production are sensitive to details of the assumed model. Besides, different choices of the analyzed reactions make difficult the comparison of results reported in various experiments.

VII. CORRELATIONS OF NONRESONANT TYPE

A. Angular-Correlation Effect (GGLP Effect)

Angular correlations between pions were first seen by Goldhaber *et al.*[37] in many-pion $\bar{p}p$ annihilations, and confirmed later in experiments at various $\bar{p}$ momenta and multiplicities, reviewed in Ref. 59.

1. *Definition of the* GGLP *Effect*

The distribution of the opening angle θ between two particles can be described by the ratio

$$\gamma = \frac{N(\theta > 90°)}{N(\theta < 90°)}$$

as proposed first in Ref. 37.

The distribution of θ, calculated in the c.m. system, is in general anisotropic: As a result of the momentum conservation there are more pairs with $\theta > 90°$ than with $\theta < 90°$. Therefore the coefficient γ is usually greater than unity. In many-pion $\bar{p}p$ annihilations the values of γ depend on the charge of the involved pions; γ^L for like pairs ($\pi^+\pi^+$ or $\pi^-\pi^-$) being smaller than γ^U for unlike pairs $\pi^+\pi^-$. This difference of γ^L and γ^U, due to correlations between pions, is usually called the GGLP effect. As a measure of the correlation, instead of the two parameters γ, one may also define the parameter[59] C:

$$C = \frac{\gamma^U - \gamma^L}{(1+\gamma^U)(1+\gamma^L)}.$$

2. *Experimental Results*

The first evidence for the presence of the GGLP effect in πp high-multiplicity collisions was found in the $\pi^+ p$ experiment at 8 GeV/c,[35] where the results based on about 40% of the present statistics were included.

It is not obvious in which reference frame one should study the angular correlations in πp collisions. In the c.m. system the peripheral emission of a secondary nucleon is reflected in the

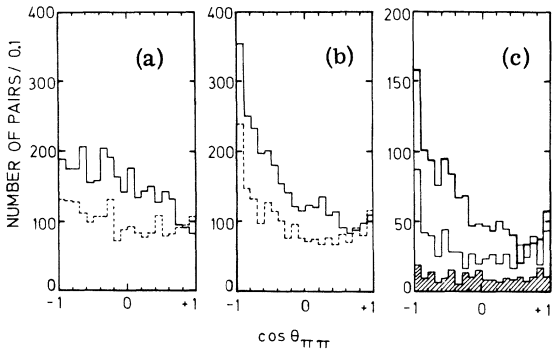

FIG. 37. Distributions of the opening angle of pairs of pions for reaction A: (a) calculated in the c.m. system: solid and dashed histograms correspond to unlike ($\pi^+\pi^-$) and like ($\pi^+\pi^+$ and $\pi^-\pi^-$) pairs, respectively; (b) The corresponding distributions calculated in the rest frame of all pions; (c) for events with smaller $\langle E \rangle$ in the rest frame of all pions: solid, thin solid, and shaded histograms correspond to the $\pi^+\pi^-$, $\pi^+\pi^+$, and $\pi^-\pi^-$ pairs, respectively.

collimation of remaining particles and affects the distributions of their opening angle. This can be avoided by using, instead of the over-all c.m. system, the rest frame of all pions.

In Fig. 37(a) the distributions are shown of the opening angle of pion pairs for reaction A, calculated in the c.m. system. Solid and dashed histograms correspond to the unlike ($\pi^+\pi^-$) and like pairs ($\pi^+\pi^+$ and $\pi^-\pi^-$), respectively. The corresponding distributions calculated in the rest frame of all pions are presented in Fig. 37(b). Comparison of Figs. 37(a) and 37(b) clearly shows the influence of a secondary nucleon on the distributions of the opening angle.

The coefficients γ and C calculated in the over-all c.m. system and in the rest frame of all pions are listed in Tables XV and XVI. In Table XVII the coefficients γ and C calculated in the rest frame of all pions are given separately for events with nucleon c.m. momentum $p^* > 1.0$ GeV/c and $p^* < 1.0$ GeV/c, 1.0 GeV/c being chosen arbitrarily.

General features of the GGLP effect in this experiment are very similar to those observed in the $\bar{p}p$ multipion annihilations[59]:

(i) For a given channel the value of the coefficient C decreases with increasing average energy per pion, $\langle E \rangle$, defined in the rest frame of all pions. The dependence can be seen in Table XVII.

(ii) The value of C depends on the reaction channel. For events with smaller $\langle E \rangle$ a large value of C is obtained for channel A, whereas in the remaining channels the value of C is much smaller (see Table XVII).

In addition, for the like pairs, we observe a difference between $\pi^+\pi^+$ and $\pi^-\pi^-$. Figure 37(c) shows the distributions of the opening angle, calculated for events of channel A with smaller $\langle E \rangle$ in the rest frame of pions: Solid, solid thin, and shaded histograms correspond to the $\pi^+\pi^-$, $\pi^+\pi^+$, and $\pi^-\pi^-$ pairs, respectively. As is seen in Table XVII, in our experiment the values of γ^{--} are systematically smaller than those of γ^{++}.

The same tendency was observed in the 5-GeV/c π^+p experiment,[22] whereas the opposite ($\gamma^{++} < \gamma^{--}$) was reported in the π^-p experiments at 16 GeV/c [15] and 7 GeV/c,[7] and also (in channel A only) at 11 GeV/c [13] and 6 GeV/c.[6] Therefore, the GGLP effect in πp interactions seems to be weaker for pions having the same charge as the beam than for those with the opposite charge. It is not clear to us whether the difference between γ^{++} and γ^{--} is due to the different behavior of π^+ and π^- (see Sec. III B). The presence of a leading pion with the same charge as the beam pion might increase the corresponding γ. However, we cannot exclude the possibility that the observed effect is due to the correlation of GGLP type, the strength of which depends on the number of pions with identical charge.

B. Principal-Axis Analysis

The so-called principal-axis analysis has been proposed[60] as a method to divide secondary particles of a given interaction into two groups which travel in the c.m. system of the collision with maximum momenta. In this way one may search for quasi-two-body reactions. If resonances are produced and their Q value is not too large, their decay products should belong to one group.

The principal axis of the jet is defined as a direction in the c.m. system for which the sum of absolute values of projections of momenta of secondary particles is a maximum.

The method was applied to a sample of 330 events of channel B. Details of this study have been published elsewhere.[34] It has been found that the principal axis is to a large extent determined by the direction of the proton momentum. Analysis of invariant-mass distributions of particles from the same group showed that the efficiency of detection of resonances ($\rho^0 \to \pi^+\pi^-$, $\omega \to \pi^+\pi^-\pi^0$, $N^{*++} \to p\pi^+$) is low.

There is an indication that for a large part of produced resonances their secondaries are contained in both groups of particles.

An attempt was made to detect possible alignment of orbital momenta of secondary particles. Such an alignment along a certain direction might result in grouping of momenta of secondaries near the plane perpendicular to this direction. No evi-

TABLE XV. Angular correlation coefficients calculated in the over-all c.m. system.

Reaction	γ^{++}	γ^{--}	γ^{L}	γ^{+-}	γ^{+0}	γ^{-0}	C
A	1.34±0.07	0.97±0.09	1.23±0.06	1.38±0.05	···	···	0.029±0.015
B	1.38±0.05	1.15±0.07	1.31±0.04	1.29±0.03	1.27±0.05	1.05±0.05	−0.004±0.009
C	1.38±0.06	1.32±0.05	1.37±0.05	1.40±0.05	···	···	0.005±0.012
D	1.22±0.04	0.97±0.06	1.15±0.04	1.28±0.03	···	···	0.026±0.010
E	1.25±0.04	1.10±0.09	1.17±0.04	1.38±0.04	···	···	0.042±0.010

TABLE XVI. Angular correlation coefficients calculated in the rest frame of all pions.[a]

Reaction	γ^{++}	γ^{--}	γ^{L}	γ^{+-}	γ^{+0}	γ^{-0}	C
A	1.58±0.08	1.38±0.13	1.53±0.074	1.82±0.08	•••	•••	0.041±0.016
B	1.57±0.06	1.40±0.09	1.53±0.05	1.57±0.04	1.53±0.05	1.61±0.07	0.006±0.010
C	1.60±0.06	1.25±0.11	1.55±0.06	1.46±0.05	•••	•••	−0.014±0.012
D	1.31±0.04	1.18±0.07	1.27±0.04	1.46±0.04	•••	•••	0.034±0.010

[a]For channel E the rest frame of all pions cannot be defined.

dence was found for such an effect.

Using Monte Carlo jets with assumed alignment, it was proved that the method is not sensitive enough to detect even quite a strong effect at our multiplicity.

VIII. CONCLUSIONS

We have analyzed high-multiplicity $\pi^+ p$ reactions, in particular, the fitted six-and seven-body channels, which at 8 GeV/c are just above the average multiplicity[61] of 5.5.

We should like to summarize some of the reaction properties discussed in the present paper.

Momentum distributions of secondaries from the studied channels strongly deviate from predictions of phase space applied to the over-all final state. These deviations may be described as due mainly to the dependence of the transition-matrix element on the squared four-momentum transfer, t, from the initial to the final proton, an idea exploited in the $F(t)$ model. The model of the $F(t)$ function, which assumes that the relativistic phase space holds for the pion subsystem only, has been shown to be quite successful at our energy and about average multiplicity.

The Chan-Łoskiewicz-Allison model, in which the multiperipheral mechanism with exchange of Regge trajectories is assumed, also gives a good description of the data. Within this model low-energy groups of secondaries are described by pure phase space and this feature of the model is compatible with our experimental data. When applied to the pionic system, it coincides with the basic assumption of the $F(t)$ model. Further studies of the main bulk of inelastic collisions at energies above 10 GeV will have to be concentrated on average-multiplicity channels (six or more particles) in which low-energy clusters of particles will presumably still play an important role.

Future progress will probably rely on the development of more refined models and a systematic collection and parametrization of the data coming from more accurate experiments. Various new features of the data, even if initially unexplained, may bring clues on dynamics of many-body reactions.

In addition to the well-known smallness of transverse momenta relative to the available phase

TABLE XVII. Angular correlation coefficients calculated in the rest frame of all pions.

Reaction	$\langle E \rangle$ (GeV)	γ^{++}	γ^{--}	γ^{L}	γ^{+-}	C
			p^* of nucleon >1 GeV/c			
A	0.420	1.32±0.11	1.24±0.17	1.28±0.09	2.07±0.12	0.112±0.022
B[a]	0.366	1.47±0.11	1.25±0.15	1.42±0.09	1.73±0.09	0.047±0.019
C	0.362	1.48±0.17	1.00±0.18	1.40±0.15	1.58±0.16	0.029±0.035
D	•••[b]	1.18±0.11	1.08±0.17	1.15±0.09	1.49±0.10	0.064±0.025
			p^* of nucleon <1 GeV/c			
A	0.550	1.80±0.13	1.50±0.18	1.72±0.10	1.66±0.08	−0.011±0.017
B[c]	0.460	1.61±0.07	1.46±0.11	1.58±0.08	1.52±0.05	−0.009±0.012
C	0.465	1.62±0.07	1.29±0.13	1.57±0.06	1.44±0.05	−0.021±0.012
D	•••[b]	1.33±0.05	1.20±0.08	1.29±0.04	1.46±0.04	0.030±0.010

[a]Coefficient $\gamma^{+0} = 1.52 \pm 0.11$, $\gamma^{-0} = 1.89 \pm 0.17$.
[b]Number of pions is unknown.
[c]Coefficient $\gamma^{+0} = 1.53 \pm 0.06$, $\gamma^{-0} = 1.53 \pm 0.08$.

space there are some other features in the distribution of this variable. Transverse momenta of secondary protons have an average of about 440 MeV/c in six- and seven-body channels and are higher for the protons emitted forwards in the c.m. system. Transverse momenta of pions are exceptionally low for pions with c.m. longitudinal momentum close to zero and for forward pions are higher than for backward ones. Furthermore, in our experiment and in most of other $\pi^+ p$ data on six- and seven-body channels, pions with the same charge as the beam have higher transverse momenta than the pions of opposite charge.

There is a small excess of positive pions with large positive values of the longitudinal momentum (leading pions), but on the average the π^+ distribution is shifted backward with respect to the π^- distribution, to the extent which can hardly be explained as a consequence of the backward N_{33}^{*++} production and its decay into p and π^+.

The GGLP effect observed in the opening-angle distributions of pairs of pions is most clearly seen in the six-body channel and enhanced by selecting events with low energy of the pionic system. This is consistent with the characteristics of the GGLP effect observed in many-pion $\bar{p}p$ annihilations. A study of these phenomena in πp interactions is obscured by the fact that single-particle distributions of π^+ and π^- are different and therefore the observed differences between pairs with various charges are not necessarily due to correlations between pion momenta.

Pions analyzed in inelastic many-body collisions are in part the decay products of various resonances. In the present experiment mesonic resonances ρ^0 and ω, the N_{33}^{*++} isobar, and such less-frequent states as η, X^0, and D^0, yield 34% of all pions produced in the six-body channel and 43% of pions in the seven-body channel with proton. The N_{33}^{*++} is observed as a final baryon in 39% of events of six-body channel and 39% of events of seven-body channel. No other nucleon isobar is clearly seen.

The average number of detected resonance combinations per event is only slightly bigger than one in channels A and B. However the associated production of resonances is considerable. The strongest effect is the simultaneous production of N^{*++} and ω which occurs in $(28.3 \pm 3.3)\%$ of the events in channel B.

The X^0 and D^0 resonances are observed in the $\eta\pi^+\pi^-$ decay channel with the cross sections of 60 ± 19 and 66 ± 17 μb, respectively. The X^0 is produced in about half of the events in association with the N_{33}^{*++} isobar and the observation of this two-body reaction allows us to derive the η^0-X^0 mixing angle using the quark model. Some evidence was presented for the decay of the D^0 meson through the intermediate $\delta\pi$ state: $D^0 \to \delta^\pm \pi^\mp \to \eta\pi^+\pi^-$.

Comparison of the data on six- and seven-body channels with lower-multiplicity data of the Aachen-Berlin-CERN Collaboration allowed us to determine the branching ratio $(f^0 \to 2\pi^+ 2\pi^-)/(f^0 \to 2\pi)$ to be $(2.2^{+4.5}_{-2.2})\%$ and the upper limit on the branching ratio $[A_{1,2} \to X^0\pi]/[A_{1,2} \to \text{(all modes)}]$ to be 2.5%.

ACKNOWLEDGMENTS

We are deeply indebted to the operating crews of the CERN proton synchrotron, the 81-cm Saclay hydrogen bubble chamber, and the CERN Track Chamber Division for providing us with the film. We would like to thank the scanning and measuring staff at our laboratory. We are grateful to Professor J. Zakrzewski for reading the manuscript and for many useful discussions and to Professor M. Danysz and Professor J. Pniewski for support and interest in this work.

---

*Deceased.

[1]R. H. Allen and V. G. Lind, Bull. Am. Phys. Soc. 13, 589 (1968).

[2]K. Abe, A. D. Johnson, V. J. Stenger, and P. G. Wohlmut, Phys. Rev. D 2, 91 (1970).

[3]R. A. Luke and V. G. Lind, Bull. Am. Phys. Soc. 13, 589 (1968).

[4]V. V. Glagolev, V. N. Emelianenko, L. I. Juravleva, R. M. Lebedev, G. D. Pestova, I. S. Saitov, J. Sedlak, V. N. Streltsev, N. P. Bogatchev, E. S. Kuznetsova, H. Böttcher, C. Grote, A. Meyer, W. D. Nowak, A. Pose, H. Schiller, and M. Walter, paper submitted to the Fifteenth International Conference on High Energy Physics, Kiev, U.S.S.R., 1970 (unpublished).

[5]F. Bomse, S. Borenstein, E. B. Brucker, A. Callahan, J. Cole, D. Ellis, D. Gillespie, G. Luste, E. Moses, A. Pevsner, and R. Zdanis, Phys. Rev. 162, 1328 (1967).

[6]K. F. Suen, E. D. Alyea, Jr., K. F. Galloway, H. J. Martin, Jr., W. E. Powers, and T. M. Small, Phys. Rev. D 1, 54 (1970).

[7]M. A. Ijaz and J. E. Campbell, Nucl. Phys. B7, 175 (1968).

[8]M. A. Ijaz and J. E. Campbell, Nuovo Cimento 61A, 307 (1969).

[9]J. E. Campbell and M. A. Ijaz, Nucl. Phys. B12, 549 (1969).

[10]P. Berenyi, J. D. Prentice, N. R. Steenberg, T. S. Yoon, and W. D. Walker, Bull. Am. Phys. Soc. 12, 684 (1967).

[11]P. Berenyi, M. S. thesis, University of Toronto, 1967 (unpublished).

[12]M. Bardadin, L. Michejda, S. Otwinowski, and

R. Sosnowski, Institute for Nuclear Research Report No. 511/VI, 1964 (unpublished).

[13]P. Daronian, A. Daudin, B. Gandois, C. Kochowski, and L. Mosca, CERN Report No. CERN-Th-68-7, 1968 (unpublished), p. 226.

[14]P. Daronian, A. Daudin, and L. Mosca, paper submitted to the Colloquium on High Multiplicity Hadronic Interactions, Paris, 1970 (unpublished).

[15]Aachen-Berlin-Bonn-CERN-Warsaw Collaboration, B. Junkmann, E. Keppel, G. Kraus, R. Schulte, R. Steinberg, C. Grote, S. Nowak, E. Ryseck, H. J. Schreiber, K. Böckmann, H. Drevermann, N. Stief, K. Sternberger, B. Wagini, K. W. J. Barnham, V. T. Cocconi, J. D. Hansen, G. Kellner, W. Kittel, D. R. O. Morrison, H. Tofte, A. Mihul, M. Bardadin-Otwinowska, T. Hofmokl, L. Michejda, S. Otwinowski, R. Sosnowski, M. Szeptycka, W. Wójcik, and A. Wróblewski, Nucl. Phys. B8, 471 (1968).

[16]F. Hamzeh, M. S. thesis, Paris University, 1965 (unpublished).

[17]D. D. Carmony, D. N. Hoa, R. L. Lander, C. Rindfleisch, and Ng. H. Xuong, paper submitted to the Twelfth International Conference on High Energy Physics, Dubna, 1964 (unpublished).

[18]Aachen-Berlin-Bonn-Hamburg-München Collaboration, L. Bondar, K. H. Eickel, H. Kaufmann, K. Lanius, R. Leiste, R. Pose, K. Böckmann, U. Gorsch, K. Steinberger, B. Nellen, V. Blobel, H. Butenschon, I. Damann, P. v. Handel, E. Lohrmann, P. Schilling, G. Wolf, N. N. Biswas, N. Schmitz, and I. Weigl, Nuovo Cimento, 44, 530 (1966).

[19]D. D. Carmony, R. L. Lander, Ng. H. Xuong, and P. M. Yager, paper submitted to the Oxford International Conference on Elementary Particles, 1965 (unpublished).

[20]Bonn-Durham-Nijmegen-Paris-Torino Collaboration, H. Drevermann, U. Idschock, K. Böckmann, A. J. Apostalakis, G. Briggs, C. A. Kitchen, J. V. Major, C. L. Pols, J. Schotanus, D. Toet, R. T. Van De Walle, R. Lestienne, P. Fleury, C. Grosso, B. Quassiati, G. Rinaudo, and A. Werbrouck, Phys. Rev. 161, 1356 (1967).

[21]U. Idschock, Bonn University report, 1967 (unpublished).

[22]R. Lestienne, Ph. D. thesis, Paris University, 1967 (unpublished).

[23]P. F. Slattery and H. L. Kraybill, Bull. Am. Phys. Soc. 11, 55 (1966), and private communication.

[24]M. Bardadin-Otwinowska, M. Danysz, T. Hofmokl, S. Otwinowski, H. Piotrowska, R. Sosnowski, M. Szeptycka, A. Wróblewski, Acta Phys. Polon. 31, 431 (1967).

[25]C. Baltay, P. Franzini, L. Kirsch, H. Kung, N. Yeh, and M. Rabin, Bull. Am. Phys. Soc. 12, 9 (1967).

[26]H. Kung, Ph. D. thesis, Columbia University, 1969 (unpublished).

[27]Chan Hong-Mo, J. Łoskiewicz, and W. W. M. Allison, Nuovo Cimento 57, 93 (1968).

[28]See, for example, O. Czyżewski, Rapporteur's talk, in *Proceedings of the Fourteenth International Conference on High Energy Physics, Vienna, 1968*, edited by J. Prentki and J. Steinberger (CERN, Geneva, 1968), p. 365.

[29]S. Otwinowski, Acta Phys. Polon. 35, 603 (1969).

[30]G. Bialkowski and R. Sosnowski, Phys. Letters 25B, 519 (1967).

[31]A. Ziemiński, Nucl. Phys. B14, 75 (1969).

[32]M. Bardadin-Otwinowska, M. Danysz, T. Hofmokl, S. Otwinowski, H. Piotrowska, R. Sosnowski, M. Szeptycka, and A. Wróblewski, Phys. Letters 21, 357 (1966).

[33]T. Hofmokl, L. Michejda, S. Otwinowski, R. Sosnowski, M. Szeptycka, W. Wójcik, and A. Wróblewski, Nucl. Phys. B4, 573 (1968).

[34]M. Danysz and W. Wójcik, Acta Phys. Polon. 33, 81 (1968).

[35]J. Bartke, O. Czyżewski, J. A. Danysz, A. Eskreys, J. Łoskiewicz, P. Malecki, J. Zaorska, K. Eskreys, K. Juszczak, D. Kisielewska, W. Zieliński, M. Szeptycka, K. Zalewski, G. Pichon, and M. Rumpf, Phys. Letters 24B, 163 (1967).

[36]M. Aderholz, M. Deutschmann, E. Keppel, G. Kraus, H. Weber, C. Grote, H. H. Kaufmann, S. Nowak, M. Walter, H. Böttcher, T. Byer, V. T. Cocconi, J. D. Hansen, G. Kellner, W. Kittel, M. Markytan, A. Mihul, D. R. O. Morrison, and H. Tofte (Aachen-Berlin-CERN Collaboration), Nucl. Phys. B8, 45 (1968).

[37]G. Goldhaber, S. Goldhaber, W. Lee, and A. Pais, Phys. Rev. 120, 300 (1960).

[38]See, for example, L. Van Hove, Nucl. Phys. B9, 331 (1969).

[39]The p_L^* distribution of π^+ for which the mass of the $p\pi^+$ system is in the interval 1.15–1.35 GeV was compared with the distribution of π^- giving $p\pi^-$ mass in the same mass band. The π^+ distribution contains both the pions from N^{*++} decay and from the background whereas the π^- distribution shows mostly the background contribution since N^{*0} production is weak. It has been verified that the two distributions are very similar. The shaded area in Fig. 10 is the p_L^* distribution of π^+ normalized to the number of N^{*++} resonance combinations.

[40]Z. Ajduk, L. Michejda, and W. Wójcik, Acta Phys. Polon. A37, 285 (1970).

[41]M. Bardadin-Otwinowska, L. Michejda, S. Otwinowski, and R. Sosnowski, Phys. Letters 21, 351 (1966).

[42]J. D. Jackson, Nuovo Cimento 34, 1644 (1964).

[43]For correction we used the values taken from Ref. 44:

$$\frac{\eta^0 \to \pi^+\pi^-\pi^0 \text{ and } \pi^+\pi^-\gamma}{\eta^0 \to \text{all modes}} = 0.29\,,$$

$$\frac{\omega \to \pi^+\pi^-\pi^0}{\omega \to \text{all modes}} = 0.9\,.$$

[44]For a review of Particle Properties see Particle Data Group, Rev. Mod. Phys. 41, 109 (1969).

[45]For correction we used the value taken from Ref. 44:

$$\frac{X^0 \to \pi^+\pi^-\eta^0 \to \pi^+\pi^-\pi^+\pi^-\pi^0(\gamma)}{X^0 \to \text{all modes}} = 0.13\,.$$

[46]S. Otwinowski, Phys. Letters 29B, 529 (1969).

[47]S. Otwinowski, Institute for Nuclear Research Report No. 1207/VI, 1970 (unpublished).

[48]For references and discussion of the D^0 and δ mesons see Particle Data Group, Rev. Mod. Phys. 42, 87 (1970).

[49]G. Ascoli, H. B. Crawley, D. W. Mortara, and A. Shapiro, Phys. Rev. Letters 21, 1712 (1968).

[50]In the Breit-Wigner formula (Sec. IV B) we used

$$\Gamma(m)=\Gamma(m_0)\left(\frac{q}{q_0}\right)^3\frac{1+q_0^2r^2}{1+q^2r^2},$$

with the value of $r=1.9$ F taken from the work of V. Alles Borelli, B. French, A. Frisk, and L. Michejda, Nuovo Cimento 48, 360 (1967).

[51]J. G. Rushbrooke, Rapporteur's talk, in *Proceedings of the Fourteenth International Conference on High-Energy Physics, Vienna, 1968*, edited by J. Prentki and J. Steinberger, Ref. 28, p. 158.

[52]We estimate that the background in the N^{*++} band is roughly compensated by N^{*++} events falling outside this band.

[53]G. H. Trilling, J. L. Brown, G. Goldhaber, S. Goldhaber, J. A. Kadyk, and J. Scanio, Phys. Letters 19, 427 (1965).

[54]For references see T. Hofmokl and M. Szeptycka, Acta Phys. Polon. 36, 929 (1969).

[55]See, for example, L. Jauneau and D. Morrellet, CERN Report No. CERN 64-13, 1964 (unpublished), presented to the 1964 Easter School for Physicists, Herceg-Novi, Yugoslavia.

[56]G. Alexander, H. J. Lipkin, and F. Scheck, Phys. Rev. Letters 17, 412 (1966).

[57]W. R. Butler, D. G. Coyne, G. Goldhaber, B. H. Hall, J. N. MacNaughton, and G. H. Trilling, Lawrence Radiation Laboratory Report No. UCRL-19225, 1969 (unpublished).

[58]E. D. Alyea, Jr., R. R. Crittenden, K. F. Galloway, K. Y. Lee, H. J. Martin, and K. F. Suen, Phys. Rev. Letters 21, 1421 (1968).

[59]O. Czyżewski and M. Szeptycka, Phys. Letters 25B, 159 (1967).

[60]S. Brandt, Ch. Peyrou, R. Sosnowski, and A. Wróblewski, Phys. Letters 12, 57 (1964).

[61]J. Bartke and O. Czyżewski, Nucl. Phys. B5, 582 (1968).